Aus der Medizinischen Klinik und Poliklinik III

Klinikum der Ludwig-Maximilians-Universität München

CRISPR/Cas9-mediated gene editing to analyze the impact of NOTCH1 mutations and their potential as a therapeutic target in mantle cell lymphoma

Dissertation

zum Erwerb des Doktorgrades der Medizin

an der Medizinischen Fakultät der

Ludwig-Maximilians-Universität München

vorgelegt von

Martine Donven

aus

Luxemburg

Jahr

2025

Mit Genehmigung der Medizinischen Fakultät der

Ludwig-Maximilians-Universität zu München

Erster Gutachter:	Prof. Dr. Martin Dreyling
Zweiter Gutachter:	Prof. Dr. Ralph Mocikat
Dritter Gutachter:	Prof. Dr. Stefan Stricker

Mitbetreuung durch den promovierten Mitarbeiter:	Dr. med. Elisabeth Silkenstedt
Dekan:	Prof. Dr. med. Thomas Gudermann

Tag der mündlichen Prüfung: 24.07.2025

CRISPR/Cas9-mediated gene editing to analyze the impact of *NOTCH1* mutations and their potential as a therapeutic target in mantle cell lymphoma

Abstract

Mantle cell lymphoma (MCL) is a rare subtype of Non-Hodgkin Lymphoma representing about 5-7% of all Non-Hodgkin lymphomas in Western Europe. Although high initial response rates can be achieved with current standard therapy, early relapses and rapid disease progression determine the clinical course of most MCL patients and prognosis is still poor with an overall survival of only 3-5 years.

NOTCH1 gene mutations occur in 5-10% of mantle cell lymphoma (MCL) and are associated with significantly lower survival rates. The majority of these mutations lead to a truncation of the PEST domain, resulting in overactivity of the Notch1-signalling pathway. However, functional relevance of *NOTCH1* mutations and its potential as a specific therapeutic target is not fully elucidated.

In this study, the CRISPR/Cas9 method was used to modify the PEST domain of the *NOTCH1* gene in the MCL cell lines Mino and Jeko-1. The aim was to establish genetically identical cell clones that differ by a single mutation in the PEST domain of their *NOTCH1* gene. These clones could further be used to perform experiments analyzing *NOTCH1* specific functions that are not confounded by intercellular differences. Additionally, the efficiency of drugs and antibodies targeting *NOTCH1* signaling could be tested on the generated cell clones.

In the Mino cell line, we attempted to repair the point mutation in the PEST domain of the gene with a homology directed repair (HDR) template, whereas in Jeko-1 cells, harboring the wildtype sequence of the gene, we aimed to introduce a point mutation in the PEST domain through non-homologous end joining (NHEJ).

For both cell lines, the introduction of the guide RNA into the CRISPR/Cas9 backbone was successful and an electroporation program was established. However, in the Mino cell line, the repair of the mutation could not be achieved as the CRISPR/Cas9 construct disrupted the growth of the cell clones. Nevertheless, a mutation was successfully introduced into the *NOTCH1* gene of the Jeko-1 cells and genetically stable Jeko-1 cell clones harboring a point mutation in the PEST domain of the *NOTCH1* gene were created. As assessed by Western Blot analysis, *NOTCH1*-mutated clones expressed a shorter Notch1 protein due to the mutation in the PEST domain leading to a truncated protein with enhanced stability upon stimulation with DLL4.

Zusammenfassung

Das Mantelzelllymphom ist eine seltene Untergruppe der Non-Hodgkin Lymphome, die etwa 5-7% aller Non-Hodgkin Lymphome in Westeuropa darstellt. Inzwischen kann durch eine Behandlung nach den aktuellen Therapiestandards initial ein hohes Behandlungsansprechen erzielt werden, jedoch ist der klinische Verlauf ebenfalls durch eine hohe Frührezidivrate und einen aggressiven Verlauf geprägt. Die Prognose von Patienten mit Mantelzelllymphom ist immer noch schlecht bei einem Gesamtüberleben von nur 3-5 Jahren.

NOTCH1 Genmutationen kommen in 5-10% der Mantelzelllymphome vor und sind mit einem signifikant reduzierten Gesamtüberleben assoziiert. Diese Mutationen führen meistens zu einer Verkürzung der PEST-Domäne, was zu einer Überaktivierung des Notch1-Signalweges führt. Die funktionale Bedeutung von Notch1 Mutationen und ihre Bedeutung als Therapieansatz ist noch nicht vollständig erforscht.

In dieser Arbeit wurde mithilfe der CRISPR/Cas9 Methode die PEST-Domäne des *NOTCH1* Gens in den Mantelzelllymphomzelllinien Mino und Jeko-1 verändert. Ziel war es, genetisch identische Zellreihen zu etablieren, die sich ausschließlich durch eine Veränderung in der PEST-Domäne des *NOTCH1* Gens unterscheiden. Diese CRISPR/Cas9 veränderten Zellen können eingesetzt werden, um die Auswirkungen einer *NOTCH1* Mutation durch Experimente zu charakterisieren, ohne die Ergebnisse durch interzelluläre Differenzen zu verfälschen. Zusätzlich kann die Wirksamkeit von *NOTCH1* Inhibitoren und monoklonalen *NOTCH1* Antikörpern an den hergestellten Zellklonen getestet werden.

In der Mino Zelllinie war das Ziel, CRISPR/Cas9 basiert die Punktmutation in der PEST-Domäne des *NOTCH1* Gens mithilfe homologer Rekombinationsmechanismen (HDR) zu reparieren, wohingegen das Ziel in der Jeko-1 Zelllinie darin bestand, eine Mutation mithilfe nicht-homologer Endverknüpfung (NHEJ) in das wildtypische *NOTCH1* Gen einzufügen.

Für beide Zelllinien ist es in dieser Arbeit gelungen, passende Guides in ein CRISPR/Cas9 Grundgerüst einzubringen. Außerdem konnte für die anschließende Transfektion mit dem CRISPR/Cas9 Konstrukt erfolgreiche Transfektionsprogramme für diese Zelllinien etabliert werden. Leider konnte in der Mino Zelllinie keine Reparatur der Mutation erzielt werden, da das CRISPR/Cas9 Konstrukt das Zellwachstum negativ beeinflusst. In den Jeko-1 Zelllinien konnte allerdings erfolgreich eine Mutation in die PEST-Domäne des *NOTCH1* Gens eingefügt werden, sodass genetisch stabile Jeko-1 Klone mit einer potenten *NOTCH1* Mutation hergestellt werden konnten. In der Westernblotanalyse zeigten die *NOTCH1*-mutierten Klone ein verkürztes Notch1 Protein aufgrund der verkürzten PEST-Domäne mit erhöhter Stabilität nach DLL4 Stimulation.

Table of contents

Figures

Tables

Abbreviations

7-AAD	7-Aminoactinomycin D
AD	*aqua destillata*
ALL	acute lymphoblastic leukemia
APS	ammonium persulfate
ASCT	autologous stem cell transplantation
ATM	*ataxia-telangiectasia mutated*
bp	base pair
BSA	bovine serum albumin
C	control
ca.	circa
CDK	cyclin-dependent kinases
cl.	cleaved
CLL	chronic lymphocytic leukemia
Co	colony
CO_2	carbon dioxide
CRISPR	Clustered Regularly Interspaced Short Palindromic Repeats
CT	computed tomography
DAPI	4′,6-diamidino-2-phenylindole
DLL4	delta-like ligand 4
DMSO	dimethyl sulfoxide
DNA	deoxyribonucleic acid
ds	double-stranded
ECOG	Eastern Cooperative Oncology Group
F	forward gRNA strand
FACS	Fluorescence-Activated Cell Sorting
FBS	fetal bovine serum
FISH	Fluorescence in situ hybridization
g	grams
GFP	green fluorescent protein
GMOs	genetically modified organisms
GSI	γ-secretase inhibitors
gRNA	guide RNA
h	hour
H_2O	water
H_2O_2	hydrogen peroxide
HD	heterodimerization domain
HDR	homology directed repair
HIV	human immunodeficiency virus
IG	immunoglobulin
IGH	immunoglobulin heavy chain
IMDM	Iscove's Modified Dulbecco's Medium
J	Jeko-1
kDa	kilodalton
LB	lysogeny broth
LDH	lactate dehydrogenase
M	Mino
mA	milliampere
MAML1	Mastermind-like 1
MCL	Mantle Cell Lymphoma
min	minute

MIPI	Mantle Cell Lymphoma International Prognostic Index
MOMP	mitochondrial outer membrane permeabilization
NHEJ	non-homologous end joining
NICD	Notch intracellular domain
NLS	nuclear localization signal
OS	overall survival
PAM	protospacer adjacent motif
PCR	polymerase chain reaction
PEST domain	proline, glutamate, serine and threonine-rich domain
PFS	progression-free survival
PI	propidium iodide
pSpCas9	Cas9 from Streptococcus pyogenes
R	reverse gRNA strand
RAM	RBP-Jk associated module domain
RB1	Retinoblastoma protein
RBP-Jk	recombination signal binding protein for immunoglobulin kappa J region
RNA	ribonucleic acid
rpm	rounds per minute
RPMI	Roswell Park Memorial Institute
RT	room temperature
s	seconds
ss	single-stranded
T	take
TALENs	transcription activator-like effector nucleases
TBS	tris-buffered saline
TEMED	tetramethyl ethylenediamine
U	untreated
UV	ultraviolet
V	volt
yOS	yearly overall survival
ZFN	zinc finger nucleases

1 Introduction

1.1 Mantle Cell Lymphoma

1.1.1 Definition and Epidemiology

The term mantle cell lymphoma (MCL) was proposed because of the growth pattern in the early stages of the disease with tumor cells colonizing the mantle zone of lymphoid follicles (1). Since the introduction of the Revised European-American classification of the International Lymphoma Study Group (R.E.A.L.-classification) in 1994, mantle cell lymphoma is regarded as a distinctive lymphoma subtype in the nowadays renowned World Health Organization classification of malignant lymphoid disorder (2).

MCL is a rare subtype of Non-Hodgkin Lymphoma representing about 5-7% of all Non-Hodgkin lymphomas in Western Europe (3, 4). The typical immunophenotype of MCL cell is usually CD20+, CD5+, CD22+, CD79b+, FMC-7+, CD23-, CD200- (5-9). MCL is characterized by its hallmark chromosomal translocation t(11;14) (q13;q32) leading to dysregulation of the cell cycle due to an aberrant overexpression of Cyclin D1 (10, 11).

The incidence of the disease has furtherly increased over the last years currently affecting 0,8/100.000 people. As MCL is most commonly found in elderly people, the incidence is at 3-4,5/100 000 per year for a population aged over 65 years (12). The median age of diagnosis is 67 years and overall, men are affected approximately 3 times more often than women (12, 13).

1.1.2 Molecular genetics

The characteristic overexpression of cyclin D1 is caused by the translocation t(11;14)(q13; q32), which leads to juxtaposition of the proto-oncogene *CCND1* coding for the cyclin D1 protein to the immunoglobulin heavy chain (IGH) enhancer (10). This causes the constitutive overexpression of cyclin D1 (14-16). Cyclin D1 forms a heterodimeric complex with CDK4/CDK6, which is responsible for the hyperphosphorylation of the tumor suppressor protein RB1 (Figure 1) (17). RB1 blocks the transcription factor E2F. E2F influences cell cycle proteins such as cyclin E which is responsible for further cell cycle action (18). When RB1 is disabled by hyperphosphorylation, E2F is no longer blocked and can proceed with the transcription of further cell cycle proteins. The cell cycle continues and is reinforced by a positive feedback loop (19). This results in a deregulation of the G1-S phase transition and the resulting multiple DNA replications lead to genomic instability (20).

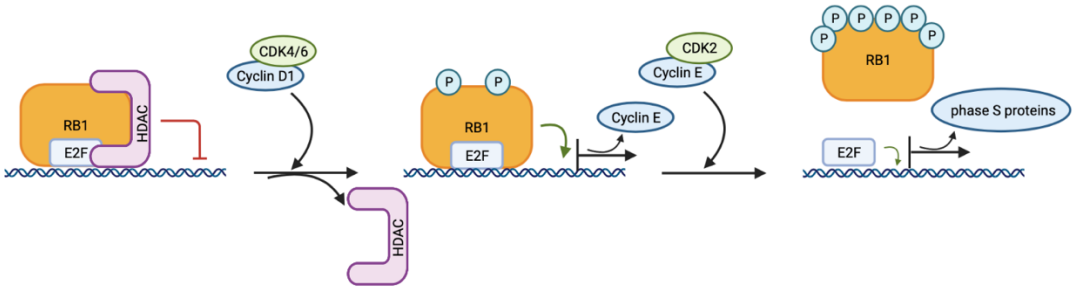

Figure 1: Simplified representation of the G1/S checkpoint regulation created with BioRender (adapted from Bertoli et al., 2013 and Malumbres et al., 2001)

A mitogenic signal induces cyclin D1 which forms a heterodimeric complex with CDK4/6. This complex induces a phosphorylation (P) of the retinoblastoma protein (RB1) and releases the histone deacetylase (HDAC). The result is in an expression of the cyclin E protein. The cyclin E/CDK2 complex hyper phosphorylates the RB1 protein which is resulting in the transcription of phase S proteins.

Yet, *CCND1* activation alone is not sufficient for a malignant cell transformation (15, 21). The most frequent mutations are the known driver mutations *TP53* (p53-inactivation), *ataxia-telangiectasia mutated* (*ATM*) and *MLL2* (22, 23). Additionally, another heterogenous group of secondary mutations influencing cell homeostasis, DNA damage response pathways or cell cycle regulation have been identified using next-generation sequencing (14, 24, 25).

In rare cases, MCL does not present a cyclin D1 overexpression or the typical *IGH/CCND1* fusion. These cancer cells show a gene expression profile typical for MCL, but the t(11;14)(q13;q32) cannot be detected. These cyclin D1 negative cases often have high expression of cyclin D2 or D3 (26). In these rare cases, the biomarker SOX-11 plays an important role in diagnosis (15, 27, 28).

1.1.3 Pathogenesis

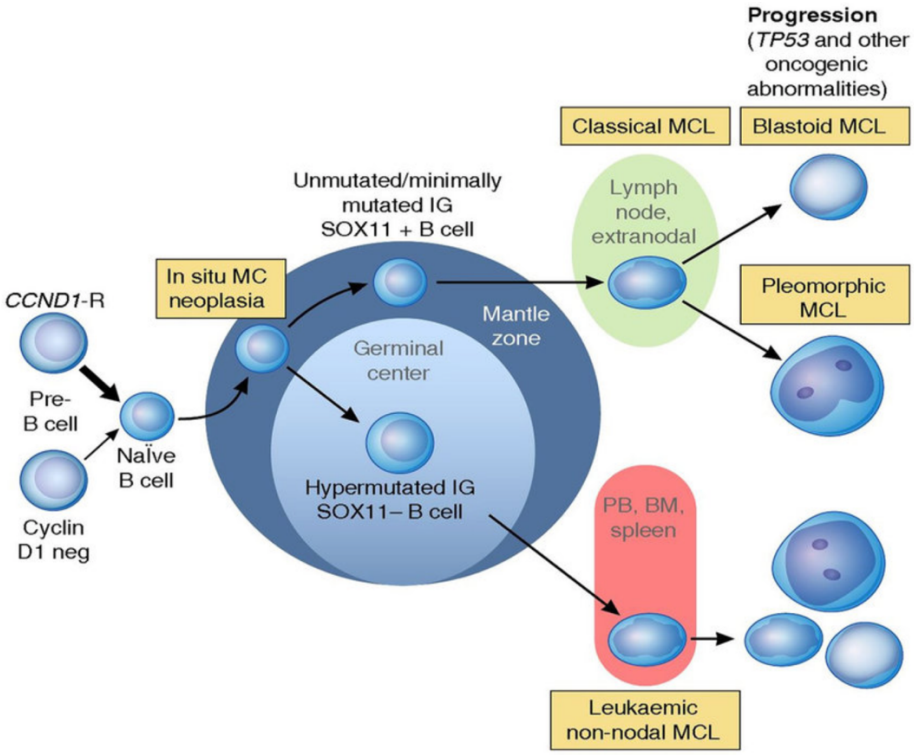

Figure 2: Proposed model of molecular pathogenesis in the development and progression of major subtypes of MCL (Swerdlow at al., 2016)

Pre-B cells, mostly carrying the typical translocation t(11;14)(q13;q32) and overexpressing cyclin D1 migrate into the mantle zone of a lymphoid follicle. MCL cells with an unmutated/minimally mutated IG and SOX-11 positivity are often genetically unstable and evolve into a classic MCL with cells migrating in lymph nodes and extra nodal locations. A progression into the more aggressive blastoid or pleomorphic MCL is possible. Sometimes MCL cells with hypermutated IG and SOX negativity pass through the germinal center of the lymph node. These cells can be genetically stable for a long time before migrating to blood, bone marrow or spleen and evolve into leukemic non-nodal MCL.

As the term mantle cell lymphoma implies, cancer cells proliferate from mature B-lymphocytes in the mantle zone of the lymph follicles (29). They can be classified as classical, small cell (B-CLL-like), pleomorphic or blastic regarding their cytological variants (Figure 2) (30). The translocation t(11;14)(q13;q32) is considered to be the primary oncogenic event in precursor B cells (31). The cells then mature into naïve B-cells. Multiple other mutations (*ATM*, *p53*, …) may occur and form an in situ MCL in the mantle zone of the lymphoid follicles. If the IG is unmutated/minimally mutated, cells often remain in the mantle zone and are SOX-11 +. They then migrate into lymph nodes or extra nodal lymph regions as classical MCL. This form is genetically unstable and can progress into the more aggressive forms like pleomorphic or blastic MCL (15, 29). The in situ MCL can also migrate into the germinal center of the lymph follicle. Under the influence of the microenvironment of the germinal center, the IG becomes hypermutated in these cells (22). They are usually SOX-11 negative and are genetically stable. This form can migrate to the spleen, bone marrow and peripheral blood and form a leukemic non-nodal MCL (29, 32).

1.1.4 Diagnostics and Staging

Usually, painless lymph node enlargement, splenomegaly or B-symptoms (fever, night sweats and weight loss) raise suspicion of a malignant disease (33). The first step is a physical examination of the Waldeyer's ring, the peripheral lymph nodes, the liver and the spleen. This examination should also be accompanied by a specifically analyzed blood sample (34, 35). A histologic analysis of a lymph node biopsy, preferably a lymph node extirpation, is indispensable. Cyclin D1 overexpression as assessed by immunohistochemistry can prove the diagnosis of mantle cell lymphoma (10). Furthermore, fluorescence in situ hybridization (FISH) analysis is recommended and can show the typical translocation t(11;14)(q13;q32). In the rare case of a cyclin D1 negative tumor, SOX-11 expression is determined (27). A bone marrow biopsy for histological examination and flow cytometry analysis can further be necessary to determine the immunophenotype of the cells (26, 35).

To determine manifestations of the disease, a computerized tomography (CT) examination of the neck, chest, abdomen and pelvis are indicated (35). Extra nodal manifestations occur in 90% of patients, including infiltration of bone marrow (53–82 %), blood (50%), liver (25 %) and the gastrointestinal tract (20–60 %) (36). MCL can also affect the central nervous system. In case of neurological symptoms, a lumbar puncture should be considered (37).

MCL is classified with the Ann-Arbor staging system (38). In stage I, cancer cells only affect a single lymph node or extra-nodal region. In stage II, at least two lymph nodes or regions on the same side of the diaphragm are affected. In stage III, cancer cells have spread to lymph nodes or regions on both sides of the diaphragm. Stage IV is characterized by a disseminated decay of at least one extra-lymphatic organ. In stage I and II, extra nodal affection is marked with "E", and in stage II, a difference between bulky and non-bulky affection in the lymph nodes is made.

1.1.5 Prognosis

Even if the prognosis of MCL has drastically improved since the introduction of therapy combinations including rituximab a couple of years ago, MCL still has a bad prognosis. The median overall survival is approximately 5 years (39).

In clinical practice, the prognosis is calculated with the MIPI (40): patients can collect a maximum of 11 points in the categories age, LDH, ECOG performance status and leucocyte count. These 4 categories were stated as independent prognostic factors for the overall survival of patients and divide the patients in low-risk, intermediate-risk and high-risk cohorts (41).

Recently, Yi et al. defined four prognostic clusters of MCL using whole-exome sequencing which showed important differences in overall survival of the subgroups. (42). The proliferation marker Ki-67 and a high *TP53* expression are mentioned to have a strong additional prognostic relevance and should be determined at first diagnosis (30, 43).

1.1.6 Therapeutic algorithm

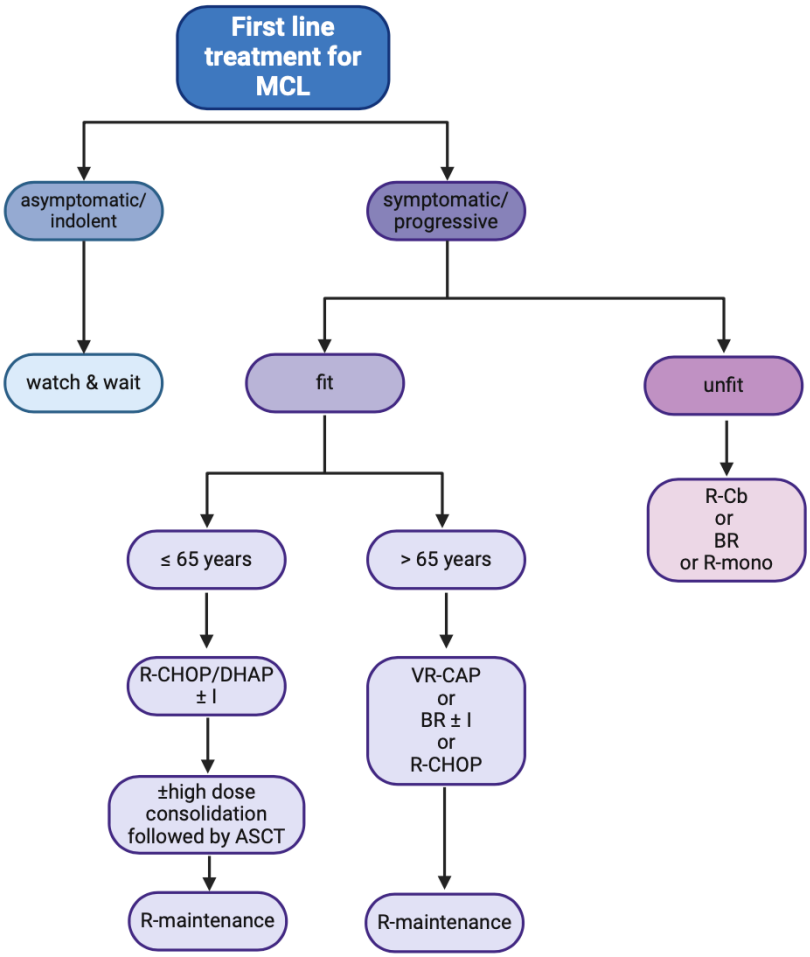

Figure 3: First line therapy algorithm for MCL patients adapted from Silkenstedt/Dreyling 2023 and https://www.onkopedia.com/de/onkopedia/guidelines/mantelzell-lymphom/@@guideline/html/index.html created with BioRender

R-CHOP: rituximab/cyclophosphamide/doxorubicin/vincristine/prednisone, R-DHAP: dexamethasone/high-dose cytarabine/cisplatin; VR-CAP: rituximab/cyclophosphamide/doxorubicin/bortezomib/prednisone, BR: rituximab/bendamustine, I: ibrutinib; R-Cb, rituximab/chlorambucil; R-mono: rituximab monotherapy; ASCT: autologous stem cell transplantation

Treatment of mantle cell lymphoma is nearly almost indicated because of the bad prognosis and the aggressive course of the disease. An exception are patients with reduced life expectancy or considerable comorbidity. These patients often receive best supportive care and if tolerated, a palliative, dose-reduced bendamustine-rituximab (BR), Rituximab/Chlorambucil (R-Cb) or Rituximab-monotherapy regimen (44). In addition, rare indolent cases can be controlled on a regular basis in terms of a so called “watch and wait” treatment. (45) In a phase II trial, Giné et al. showed that a frontline ibrutinib-rituximab regimen could have a positive influence on indolent MCL (46).

For younger patients (≤65 years), the actual standard of care consists in an induction therapy with a dose-intensified immunochemotherapy (R-CHOP/R-DHAP regimen) +/- ibrutinib (35, 47) followed by a high-dose consolidation therapy followed by an autologous stem cell transplantation (ASCT) (48, 49). The role of ASCT in ibrutinib containing regimens is currently inquired (NCT02858258, (50)). Moreover, adaptation of intensive

chemotherapy in frontline therapy according to TP53 mutation status should be considered (51). As maintenance therapy for young patients, rituximab over two years improves PFS and OS and represents the current therapy standard (52).

Elderly patients (≥ 65 years) often do not qualify for dose-intensified immunochemotherapy because of co-morbidities and their reduced performance status. (53) Therefore, they should be treated with rituximab in combination with conventional chemotherapy doses. Currently, a combination of bortezomib, rituximab, cyclophosphamide, doxorubicin and prednisone (VR-CAP) is the most promising therapy regimen. (54) For very fit old patients a combination of rituximab, bendamustine and cytarabine (R-BAC) is an alternative, although it showed severe toxicity (55). In unfit elderly patients, a bendamustine-rituximab (BR) regimen should be considered (56). Furthermore, a combination of the BR regimen with ibrutinib showed a significant improvement of PFS (52.9 to 80.6 months), however no difference on OS (44). For maintenance therapy in elderly, rituximab monotherapy also shows good results. (57)

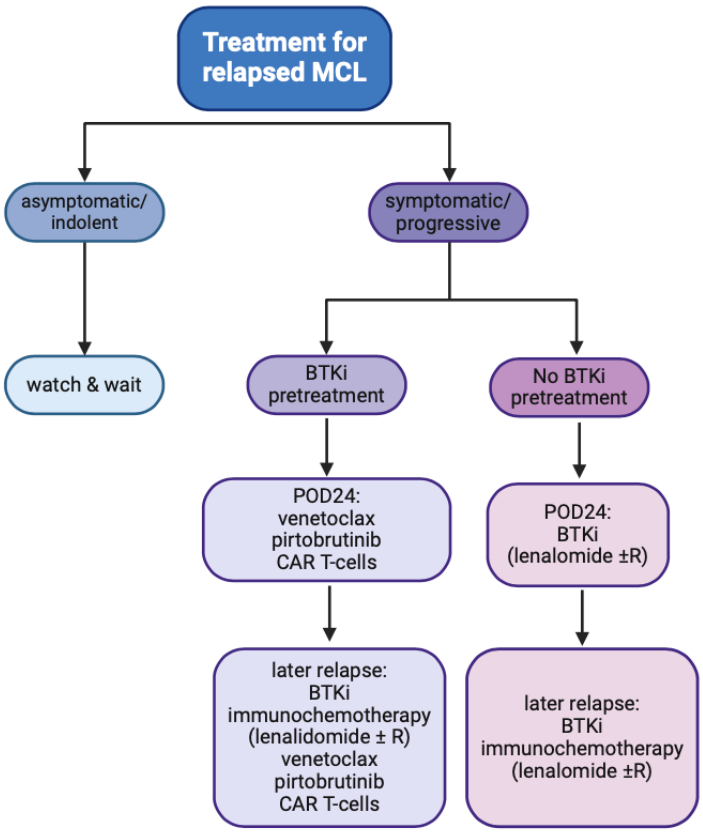

Figure 4: Therapy algorithm for relapsed MCL patients adapted from Silkenstedt/Dreyling 2023 and https://www.onkopedia.com/de/onkopedia/guidelines/mantelzell-lymphom/@@guideline/html/index.html created with BioRender

POD24: progression of disease <24 months, BTKi: Bruton´s tyrosine kinase inhibitor, chimeric antigen receptor

In case of an early relapse, another immunochemotherapy regimen or a newer targeted therapy approach should be considered. Currently, ibrutinib, a Bruton's tyrosine kinase inhibitor (BTKi), shows a high response rate and durable efficacy in relapsed and refractory mantle cell lymphoma (58). However, therapy response to ibrutinib is very heterogeneous and *TP53* mutations are associated with worse outcome. (59) Furthermore, second generation BTKi, such as acalabrutinib (NCT02972840) and zanubrutinib (NCT04002297) or next-generation BTKi pirtobrutinib (NCT04662255) show promising

results in clinical studies. In case of relapse under BTKi, other alternatives or combinations with BCL2-inhibitor venetoclax (60) or lenalidomide (61) are currently compared as targeted therapy regimens in relapsed and refractory mantle cell lymphoma. Allogenic stem cell transplantation should only be discussed in younger patients (62) after chimeric antigen receptor (CAR) T-cell therapy. In patients with *TP53* mutation, CAR T cell therapy may even be considered as second-line therapy (63, 64).

1.2 The Notch1 pathway

1.2.1 Overview of NOTCH receptors and ligands

The Notch1 receptor is one of 4 mammalian Notch receptors (Notch1-4), which are each coded by a different gene (Figure 5). Notch receptors are activated by the binding of ligands that are expressed on the surface of neighbor cells and belong to two families: Delta-like ligands (DLL1, -3, -4) and Serrate-like ligands (Jagged 1 and 2) (65).

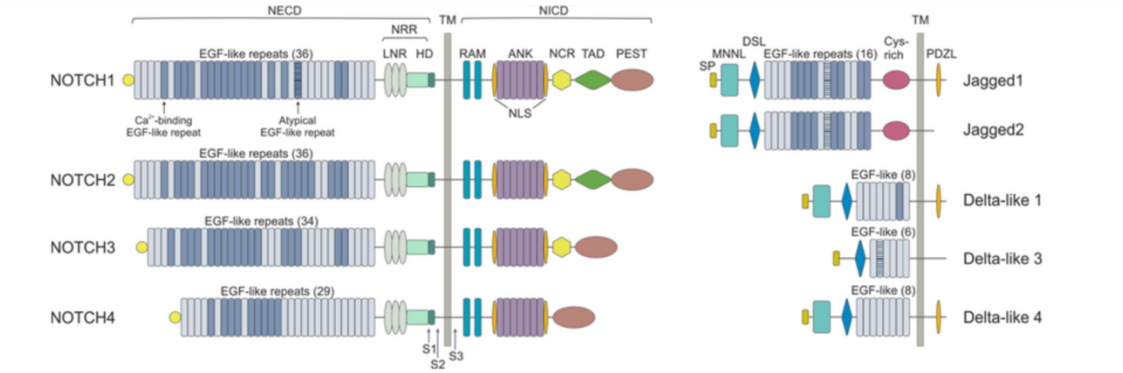

Figure 5: NOTCH receptors and ligands (Arruga et al., 2018)

ANK: ankyrin repeats domain; Cys-rich: cysteine-rich domain; DSL: Delta/Serrate/LAG-2 domain; EGF-like repeats: epidermal growth factor-like repeats; HD: heterodimerization domain; LNR: cysteine-rich Lin repeats; MNNL: NOTCH ligand N-terminal domain; NCR: NOTCH cytokine response; NECD: Notch extracellular domain; NICD: Notch intracellular domain; NLS: nuclear localization sequences; NRR: negative regulatory region; PDZL: post-synaptic density protein ligand domain; PEST: proline-glutamic acid-serine-threonine rich domain; RAM: RBP-Jk associated module domain; S1, S2, S3: cleavage sites for metalloproteases and γ-secretase; TAD: transactivation domain; TM: transmembrane domain

The Notch1 receptor is a transmembrane protein. After ligand-binding, it is activated by two cleavage steps (66). The alpha-secretase complex (ADAM10, metalloprotease) is responsible for the first, extracellular cleavage (67). The following cleavage is the intracellular cleavage. It is performed by the gamma-secretase complex, which releases the active NICD (Notch Intracellular Domain) (68). The NICD displaces co-repressor molecules bound to RBP-Jk (Recombination signal binding protein for immunoglobulin kappa J region) (69) and recruits coactivators like MAML1 (Mastermind-like 1) and p300 (histone acetyl transferase). The so formed complex influences gene expression and plays an important role in cell differentiation, cell development, cell cycle progression and apoptosis (70). In context of hematopoiesis, the Notch pathway influences the lineage specification (69, 71).

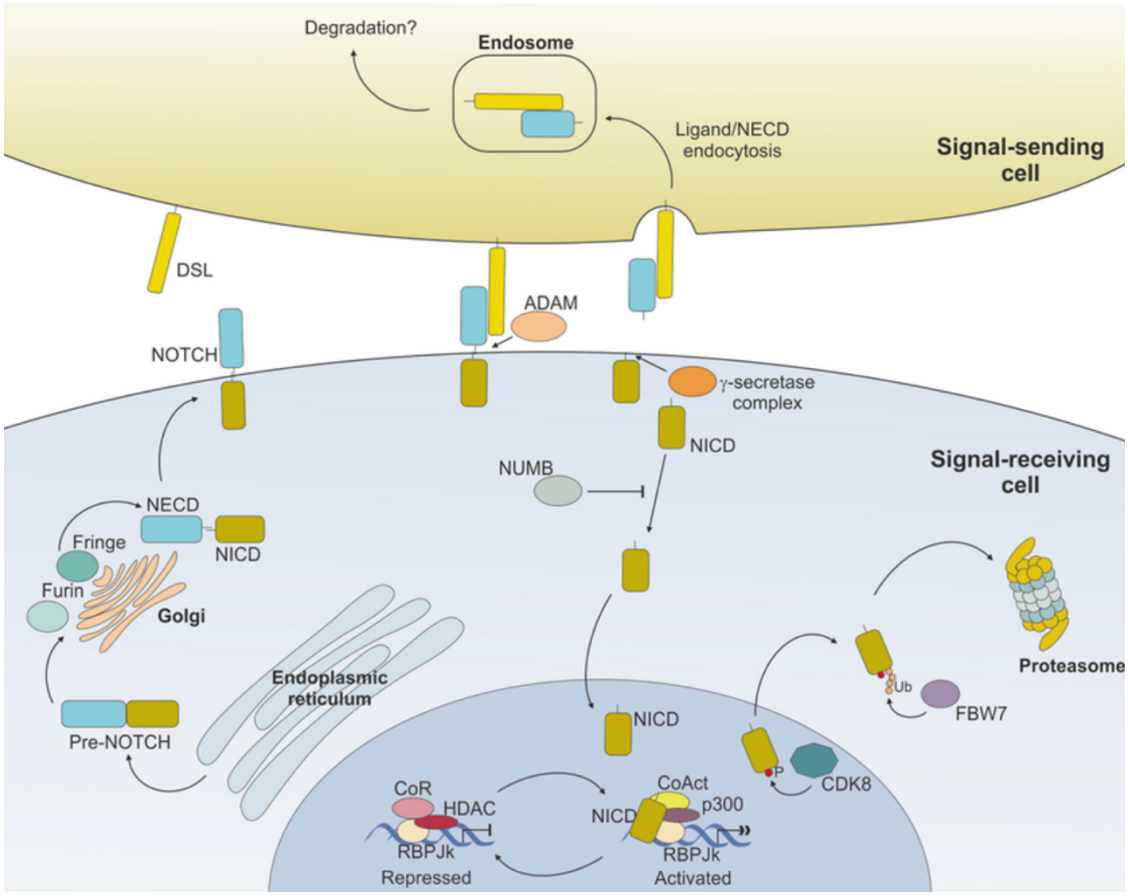

Figure 6: The Notch pathway (Arruga et al., 2018)

The development of the Notch receptor includes its maturation in the Golgi complex. The bipartite protein with an extracellular and intracellular domain is incorporated in the extracellular membrane as transmembranous receptor.
After ligand stimulation, the ADAM10 cleaves the extracellular part of the transmembrane Notch protein. The second, intracellular cleavage is performed by the gamma-secretase complex. The NICD influences gene expression and other various processes.
The degradation of the protein starts with its phosphorylation by CDK8. Subsequently, it is poly-ubiquitinated by FBW7 and degraded by the proteasome.
ADAM: A disintengrin and metalloprotease; NECD: Notch extracellular domain; NICD: Notch intracellular domain; CoR: co-repressors; HDAC: Histone Deacetylase Complex; CoAct: RBP-Jk recruiting co-activators; CDK8: Cyclin-dependent kinase 8; FBW7: F-box containing protein

In order to degrade active NICD, it is first phosphorylated by CDK8. This phosphorylated complex is afterwards recognized and poly-ubiquitinated by FBW7. The poly-ubiquitinated NICD is then degraded by the proteasome. As it was shown in previous studies, the poly-ubiquitination by FBW7 especially depends on the PEST domain of NICD. In case of mutations in this region, the poly-ubiquitination is affected and therefore, the degradation efficiency of active NICD is decreased. This results in a longer activation of Notch signaling (72).

1.2.2 *NOTCH1* molecular genetics and mutations

The extracellular part of the Notch1-receptor consists of epidermal growth factor (EGF) -like repeats for ligand interaction, LIN12/Notch repeats and a heterodimerization domain (HD) to prevent ligand-independent activation. The NICD contains the RAM-domain, nuclear localization signal (NLS), ankyrin repeats and the transactivation domain (TAD) (70, 73). The PEST domain, a proline-, glutamate-, serine- and threonine-rich domain, is

located at the C-terminal of the protein and its phosphorylation and subsequent poly-ubiquitination is responsible for degradation of the Notch1 protein by the proteasome and therefore protein stability (74).

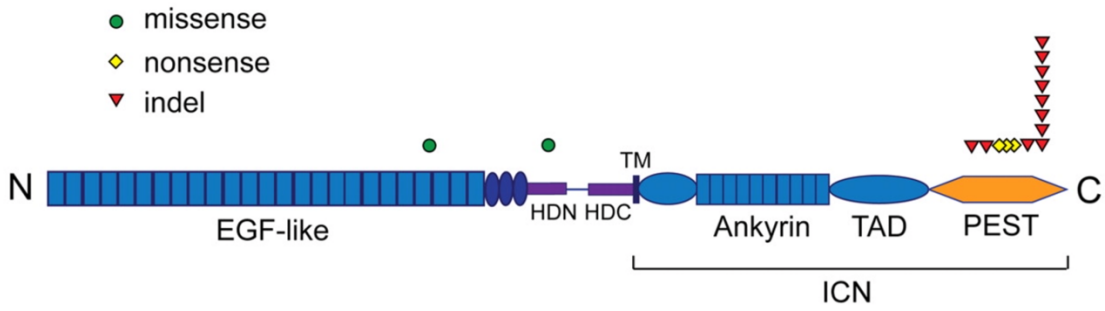

Figure 7: The most common *NOTCH1* mutations in MCL (Kridel et al., 2012)

The most common NOTCH1 mutations are found in the PEST domain of the gene. A mutation in the PEST domain often results in an increased stability of the Notch1 protein, as the protein is not recognized by the proteasome for degradation.
EGF-like epidermal growth factor-like repeats; HDC: C-terminal heterodimerization domain; HDN: N-terminal heterodimerization domain; ICN: intracellular Notch1; PEST: proline-glutamic acid-serine-threonine rich domain; TAD: transactivation domain; TM: transmembrane domain

The majority of *NOTCH1* mutations are located in the PEST domain (exon 34) and are mostly frameshift or nonsense mutations (75). They result in a truncated Notch1 protein with increased stability because of the lack of hyperphosphorylation and poly-ubiquitination (72, 74). Other mutations target the HD domain in the extracellular part of the Notch1 receptor and result in its ligand-independent activation (76).

1.2.3 The influence of *NOTCH1* mutations on prognosis

NOTCH1 mutations were described as a negative prognostic factor in MCL leading to shorter survival rates (3-yOS: 33% vs 60%, p=0,026) (22, 75). In univariate analysis, *NOTCH1* mutations were significantly associated with poorer outcome. (51) Moreover, it was shown that *NOTCH1* mutations are predominantly found in more aggressive MCL subtypes (77).

Apart from *NOTCH1* mutations in MCL, activating mutations in the Notch1 pathway also influence other hematological malignancies. For instance, it is known that *NOTCH1* gene mutations are among the most common mutations in chronic lymphocytic leukemia (CLL) and lead to a progressive disease in CLL patients (78-80). Furthermore, in human T-ALL, above 50% have activating *NOTCH1* mutations (81).

Additionally, *NOTCH1* mutations play a role in solid cancers like prostate cancer, breast cancer, colorectal cancer and melanoma (82-85).

1.2.4 *NOTCH1* as a therapeutic target in cancer

As described in section 1.2.3, *NOTCH1* mutations are known to correlate with a negative prognosis in hematological malignancies, as well as in solid cancers. Targeting *NOTCH1* has therefore become a promising therapeutic strategy in *NOTCH1* mutated cancers (86).

A first approach of *NOTCH1* targeted therapy was the use of γ-secretase inhibitors (GSI), which inhibit the second cleavage step in the Notch1 activation pathway and impede the release of active NICD. GSIs are already widely researched in T-ALL and CLL but showed severe gastrointestinal side effects in a high-dosed monotherapy. However, they showed good effects when used low-dosed in combination therapies (87, 88). Moreover, ADAM10 inhibitors, targeting the first, extracellular cleavage step of the Notch1 receptor, showed promising therapeutic effects in T-ALL (89). Additionally, Anti-*NOTCH1* antibodies such as OMP-52M51 (Brontictuzumab) or MAb604.107 are also in development in T-ALL (90, 91).

In MCL, Kridel et al. analyzed the negative prognostic effect of *NOTCH1* mutations in MCL patients, as well as *NOTCH1* mutations as a potential therapeutic target (75). Silkenstedt et al. also identified *NOTCH1* mutations as a potential therapeutic target for a specific antibody therapy with Brontictuzumab, *in vitro* and *in vivo* (92).

1.3 CRISPR/Cas9 system

1.3.1 The role of the CRISPR/Cas9 system in bacteria

The CRISPR (Clustered regularly interspaced short palindromic repeats)/Cas9 system plays an important role in the adaptive immune system of bacteria and archaea as a defense mechanism against viruses and plasmids (93, 94).

It consists of two components: the CRISPR-associated endonuclease (Cas-protein) and the guide RNA (gRNA) (95). The gRNA is composed of a scaffold sequence necessary for Cas-binding and a user-defined spacer (20-25nt) that defines the unique, genomic target. The protospacer adjacent motif (PAM) serves as a binding signal for the Cas-protein on the target DNA. Near the PAM sequence, a double strand break within the target DNA is introduced. This double-strand-break is then mended by the non-homologous (NHEJ) pathway or the homology directed repair (HDR) pathway (96).

1.3.2 The CRISPR/Cas9 system as a scientific method

The first documentation of the CRISPR/Cas9 method was published in 2012 by Emmanuelle Charpentier and Jennifer Doudna of the University of California, Berkeley (97). They earned the Nobel prize for chemistry in October 2020 for their scientific breakthrough. The CRISPR/Cas9 system, also known as “genetic scissors”, replaces the more complicated method of zinc finger nucleases (ZFNs) (98) and transcription activator-like effector nucleases (TALENs) (99). Genomes can now be edited precisely and at low cost. The team around Feng Zhang proved in 2013 that CRISPR worked in mammalian cells (95). The method is not specific for the medical field, but also used in agriculture or for creation of genetically modified organisms (GMOs) (100-103). The use of CRISPR/Cas9 in human germline to create “designer babies” is highly controversial (104-107).

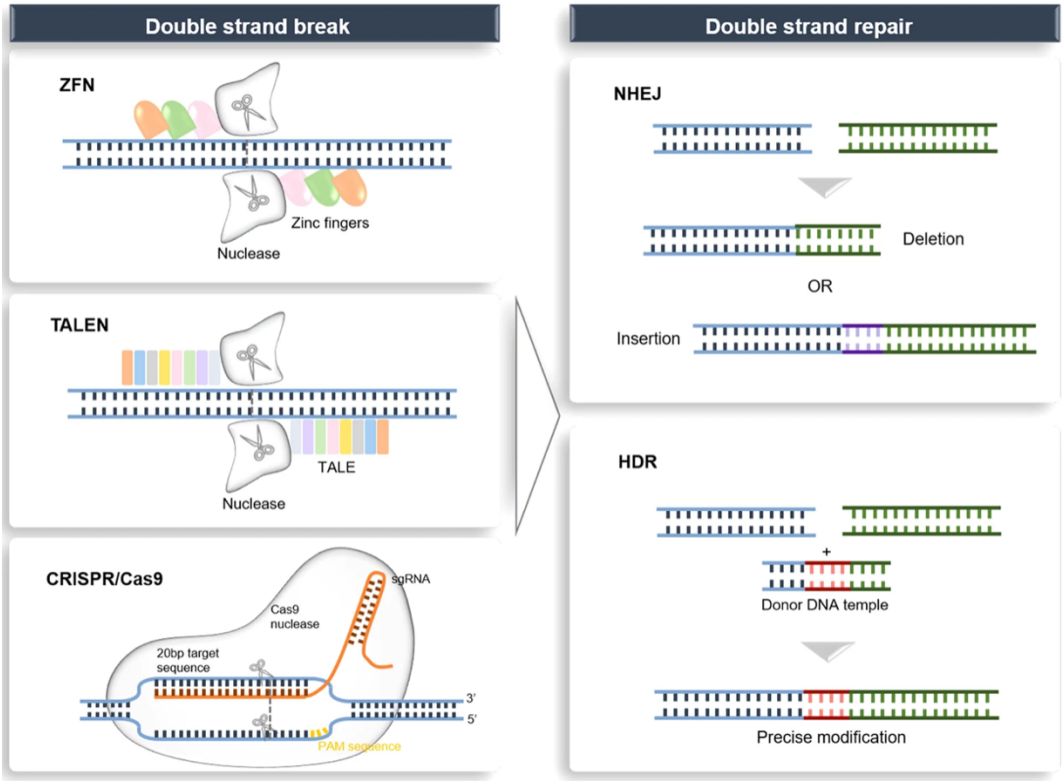

Figure 8: Genome editing methods and DSB repair mechanisms (Hongyi et al., 2020)

To create a double strand break in the DNA, the ZFNs, TALENs or the CRISPR/Cas9 method can be used. The CRISPR/Cas9 method has the benefit that the DSB can be introduced at a very specific locus in the DNA. The DSB is most frequently repaired by NHEJ, which introduces random mutations in the genome of the targeted cell. With HDR, precise modification with a donor DNA template can be achieved.
DSB: double strand break; HDR: homology directed repair; NHEJ: non-homologous end joining; sgRNA: scaffold RNA; TALEN: transcription activator-like effector nucleases; ZFN: zinc finger nucleases

The CRISPR/Cas9 targets a specific, predetermined DNA sequence and causes a double strand break. The damaged DNA sequence can be repaired by two pathways: NHEJ or HDR (108). NHEJ is the more efficient, but also the more error-prone pathway: it can lead to random deletions or insertions that disrupt or modify gene functionality (109, 110). HDR is less efficient but repairs the DNA with help of a homologous repair DNA template in order to maintain genomic stability (109). The template can be an endogenous (homologous chromosome, sister chromatid), but also an exogenous designed repair template that allows to do precise changes in the DNA (111).

The greatest concern about the CRISPR method is its precision (112, 113). Even if the precision is better than with the precursor methods in gene editing, unpredictable OFF-target breaks can be an issue. OFF-target activity can lead to irreversible changes in the genome, resulting in reduced fitness and functional impairment, or it can even induce oncogenic potential (114). It also must be considered that an introduced change in the DNA is now part of the cells genome and is passed on to the daughter cells.

1.3.3 CRISPR/Cas9 editing in the medical field

Gene editing with CRISPR/Cas9 has become very important in a wide field of genetic diseases and underwent a large development over the last few years. A crucial point for genome editing is that the patient only benefits if the edited cells gain a relative survival advantage on the diseased, non-edited cells (96).

Cells of the hematopoietic system are favorable for gene editing as they show a high editing efficiency and a good survival of cells ex vivo (96). A lot of different hematopoietic diseases, such as beta-thalassemia (115), sickle-cell disease (116) and hemophilia (117) are in research for gene editing therapy. The complications of the diseases can be drastically reduced, and they could even potentially be cured with help of the CRISPR/Cas9 method.

Another large field for the use of the CRISPR/Cas9 method is cancer research. It is currently used in attempt to edit T-cells in a way that they attack cancer cells (118). In order to do so, T-cells from the patient are genetically altered ex vivo before being retransferred into the patient. Clinical trials are performed on a various number of different cancers, such as non-small cell lung cancer (NCT02793856) (119, 120), esophageal cancer patient (NCT03081715), B-cell lymphoma and leukemia (NCT03166878). Chimeric antigen receptor (CAR) T-cell therapy have recently been approved for relapsed lymphomas and leukemia and allow personalized cancer immunotherapies (121-123). Although, under CAR T-cell therapy, cytokine release syndrome (CRS), secondary malignancies and immune cell-associated neurotoxicity syndrome (ICANS) can occur as severe side-effects (124, 125). Furthermore, CRISPR advances cancer drug research as it can be used to develop specific cell lines on which specific cancer drugs can be tested. (118)

CRISPR/Cas9 can also be employed for antimicrobial or antiviral use. An example here fore is an attempt in treatment of patients infected with HIV. The goal is to generate a T-cell population resistant to HIV infection. Therefore, a bi-allelic mutation of the gene CCR5, which is the key co-receptor for HIV entry, must be introduced to generate a HIV-resistance (126). Another potential option is to disrupt the HIV-1 provirus (127).

Furthermore, Duchenne muscular dystrophy, another disease with fatal course, could potentially be altered with CRISPR/Cas9 (128). In this disease, different mutations, most commonly a frameshift mutation, leads to a complete loss of protein functionality. The strategy here is benefitting from NHEJ-mediated genome editing and using CRISPR/Cas9 to create insertions or deletions restoring the original frameshift and therefore protein functionality (129). Another attempt is to modify the dystrophin gene in order to obtain a partially functional dystrophin protein. This is executed by knocking out exon 45-55, as the disease then takes a less severe course (130, 131).

2 Objectives

The objective of this study was the modification of the PEST domain in the *NOTCH1* gene with the CRISPR/Cas9 method in order to directly compare mutated and wildtype cells within a cell line in different biological assays. The advantage of comparing cell clones to wildtype cells rather than comparing mutated and wildtype *NOTCH1* cell lines is that intercellular differences and potentially other mutations do not interfere with analysis. Therefore, the isolated effect of *NOTCH1* can be characterized.

In this study, we used two different cell lines: Mino and Jeko-1. The Mino cell line carries a mutation in the *NOTCH1* gene (Exon 34, C>T, amino acid Q2487*) that leads to an early stop codon and consequently to a truncation of the PEST domain. This affects the degradation of the Notch1 protein and leads to an excess of Notch1 protein in the cell. Therefore, our aim for the Mino cell line was the introduction of a CRISPR/Cas9-mediated targeted double strand break and the repair of the mutation to the gene's wildtype sequence by using a customed HDR template. This should result in a wildtype Notch1 protein expression clone that can be compared with the unedited Mino cell line. On the other hand, the Jeko-1 cell line is already a carrier of the wildtype NOTCH1 gene. Therefore, our aim for these cells was to introduce a CRISPR/Cas9-mediated random mutation in the PEST domain leading to a truncated protein. Due to the truncation, the recognition of the Notch1 protein by the proteasome would be limited and therefore lead to a decreased protein degradation. This should result in a Notch1 protein excess in Jeko-1 clones.

Mino and Jeko-1 cells should subsequently be compared to their CRISPR/Cas9 edited cell clones in functional assays such as viability and proliferation assays, apoptosis induction assays, Colony-Forming-Units-Assay and angiogenesis assays. Furthermore, the effect of specific *NOTCH1* targeted therapies in mutated cells should be analyzed.

3 Materials and Methods

3.1 Materials

3.1.1 Mammalian cell lines

The important characteristics of mammalian cell lines are listed in Table 1 (132-134). The mantle cell lymphoma cell line Mino shows a point mutation in Exon 34 that changes the amino acid glutamine (Q) into a stop codon as pictured in Figure 9. This results in a truncated and dysfunctional Notch1-protein as described in section 1.2.2 . The Jeko-1 cell line on the other hand presents a wildtype *NOTCH1* gene and therefore a normally functional Notch1 protein.

Table 1: Characterization of Mantle Cell Lymphoma cell lines after DSMZ homepage (Lai et al., 2002, Jeon et al., 1998 and Amin et al., 2003)

	Mino	**Jeko-1**
Cat. No.	ACC 687	ACC 553
brand	DSMZ – German Collection of Microorganisms and Cell Cultures GmbH	
cell type	mantle cell lymphoma	mantle cell lymphoma
doubling time	ca. 50 hours	ca. 50 hours
molecular genetics	t(11;14)(q13;q32) overexpression of Cyclin D1 (*CCND1*)	*CCND1-IGH* influenced by complex chromosomal aberrations, without t(11;14)(q13;q32) overexpression of Cyclin D1 (*CCND1*)
overexpressed	Rb	Rb, c-myc, bcl-2
p53	overexpressed (mutated)	wild type
***NOTCH1* gene**	mutated Exon 34, C>T, amino acid Q2487*	wild type gene
Notch1 protein	truncated protein	wild type protein

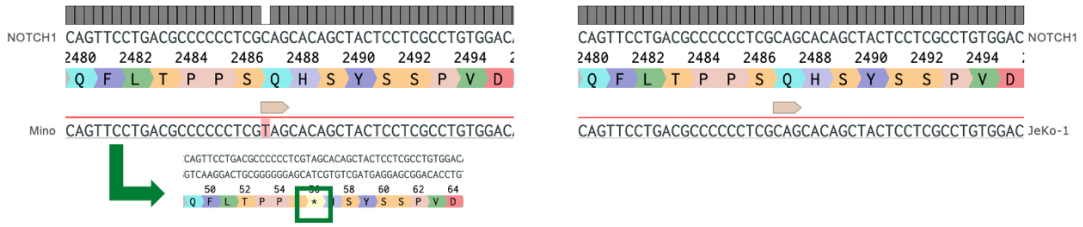

Figure 9: *NOTCH1* mutation (Exon 34, C>T, amino acid Q2487*) in PEST induces stop codon in the Mino cell line

A mutation in the PEST domain of the NOTCH1 gene in the Mino cell line changes the amino acid glutamine (Q) into a stop codon. The translation of the Notch1 protein stops preliminary and is truncated. The Jeko-1 cell line corresponds with the wildtype of the NOTCH1 gene. This figure was created with Benchling.

3.1.2 Bacterial strain

The bacterial strain was provided by Life Technologies GmbH.

Table 2: Bacterial strain

Product	bacteria	Catalogue No.	Lot No.
One Shot™ TOP10 chemically competent E. coli	E. coli D5Ha	C404003	2115520

3.1.3 Cell culture

Table 3: Cell Culture Products

Product (storage)	Article/Cat. No.	Brand
RPMI 1640 (4°C)	P04-16500	PAN™ Biotech
IMDM (4°C)	P04-20450	PAN™ Biotech
FBS Standard (4°C, -20°C)	P30-3306	PAN™ Biotech
DMSO (Dimethyl Sulfoxide) for cell culture (RT)	A3672,0100	AppliChem GmbH
AntiAnti 100x (4°C, -20°C)	REF 15240-096	gibco
Vi-Cell™ Cleaning Agent (RT)	REF 175594	Beckman Coulter
Vi-Cell™ Buffer Solution (RT)	#383202	Beckman Coulter
Vi-Cell™ 0,4% Trypan blue in NaCl (RT)	#383200	Beckman Coulter
Vi-Cell™ Disinfectant (RT)	#383201	Beckman Coulter
Recombinant Human DLL4 His-tag 50µg, reconstituted at 200µg/mL in PBS (-80°C)	#Q9NR61	R&D systems® a bio-techne® brand

3.1.4 Buffers and solutions

Buffers and solutions were stored at room temperature if not indicated otherwise.

Table 4: Buffers and Solutions

Product	compounded from	Quantities
1,5M Tris-HCl (pH 8,8/6,8)	AD Tris (pH was adjusted with HCl)	5000 mL 908,55 g
BSA 5% (4°C)	Albumin Fraction V (Roth 8076) TBST Sodium azide	5 g 100 mL Spatula tip
ECL	SA SB H_2O_2	3 mL 0,3 mL 0,9 µL
Electrophoresis Buffer 10x	Tris Glycine sodium dodecyl sulfate AD	151,4 g 720,7 g 50,0 g 5000 mL
FACS solution	Hanks' Salt Solution HEPES buffer (25mM, pH 7,0) 5% Newborn Calf Serum	462 mL 12,5 mL 25 mL
Freezing medium (4°C)	FBS Standard DMSO	46 mL 4 mL

G-NET	gelatin 10x NET AD	1,25 g 50 mL 450 mL
Gel-transfer-buffer for Western blot	Tris Glycine Methanol AD	15,0 g 71,0 g 790,0 g 5000 mL
LB-Agar	LB-Agar (Lennox) AD	17,5 g 500 mL
LB-Medium	LB Broth (Lennox) AD	10 g 500 mL
Milk 5%	Powdered milk TBST	5 g 100 mL
Protein lysis buffer	Lysis-M reagent Complete, Mini Protease Inhibitor Cocktail Tablets	10 mL 1 tablet
SA (4°C)	Luminol sodium salt 1,5M Tris pH 8,8 AD	100 mg 26,67 mL 373,3 mL
SB (light protected)	p-Coumaric Acid DMSO	44 mg 40 mL
TBS, pH 8,0 10x	Tris Sodium chloride AD (pH was adjusted with HCl)	60,57 g 483,3g 5000 mL
TBST	AD 10x TBS (pH 8,0) Tween® 20	4,5 L 500 mL 5 mL

3.1.5 Reagents

Table 5: Reagents

Product	Cat. No.	Producer
100bp DNA Ladder	REF G210A	Promega
2-Propanol 70% Art. No. CN09.2	67-63-0	Carl Roth GmbH + Co KG
2-Propanol for molecular biology	67-63-0	AppliChem GmbH
Agarose NEEO ultra-quality	2267.3	Carl Roth GmbH + Co. KG
Albumin Fraction V	8076.4	Carl Roth GmbH + Co. KG
Ampicillin	329824407	Roche
Ammonium persulfate (APS)	248614	Sigma Aldrich
BD Pharmingen™ Propidium Iodide Solution (50µg/mL, 4°C)	51-66211	BD Biosciences
Bio-Rad Protein Assay Dye Reagent Concentrate	7664-38-2	Bio-Rad Laboratories
Blue/Orange Loading Dye 6x (DNA)	REF G190A	Promega
cOmplete Tablets, Mini, EDTA-free, EASYpack (4°C)	04693159001	Roche

4′,6-Diamidino-2-phenyl-indol -dihydrochloride (DAPI)	10236276001	Roche
DMSO, ACS >99,9%	472301-1M-L	Sigma Aldrich
Electrophoresis Buffer 10x	L20200227-05	Pharmacy of Großhadern Clinic
Ethanol 70% (LAB)	64-17-5	CLN GmbH
Ethanol absolute for analysis	64-17-5	Merck KGaA
Gelatin	1.04070.	Merck KGaA
Hanks' Salt Solution	L2045	Biochrom GmbH
Hydrogen peroxide solution (H_2O_2)	216763-100ML	Sigma Aldrich
Ingenio® Solution	MIR 50117	Mirus
LB Broth (Lennox)	X964.1	Carl Roth GmbH + Co. KG
LB-Agar (Lennox)	X965.1	Carl Roth GmbH + Co. KG
LDS Sample Buffer 4x	REF B0007	Novex® by life technologies™
Luminol sodium salt	A4685-5G	Sigma Aldrich
Lysis-M Reagent	REF 04719964001	Roche Diagnostics GmbH
Methanol	8388.5	Carl Roth GmbH + Co KG
N, N, N', N'-Tetramethyl ethylenediamine (TEMED)	T7024-25ML	Sigma Aldrich
NET 10x pH 7,7	L000999	Pharmacy of Großhadern Clinic
p-Coumaric Acid	C9008-5G	Sigma Aldrich
PBS Dulbecco	L1825	Biochrom GmbH
peqGOLD Protein V	27-2210	VWR International
Phosphatase Inhibitor Cocktail 2	P5726-1ML	Sigma Aldrich
Phosphatase Inhibitor Cocktail 3	P0044-1ML	Sigma Aldrich
pmaxGFP™ 0,5µg/µL	VDC-1040	Lonza
Powdered milk	T145.2	Carl Roth GmbH + Co. KG
PureLink™ RNase A (100µg/mL)	REF 12091-021	Thermo Fisher Scientific
Rotiphorese® Gel 30	3029.1	Carl Roth GmbH + Co. KG
S.O.C medium	REF 15544-034	Invitrogen by Thermo Fisher Scientific
Sample Reducing Agent 10x	REF B0009	Novex® by life technologies™
Sodium azide	K305	Carl Roth GmbH + Co. KG
SYBR® Safe DNA Gel Stain	S33102	Invitrogen™ by life technologies™
Tris-HCL-buffer 1,5mol/L pH 6,8	L20180409-06	Pharmacy of Großhadern Clinic

Tris-HCL-buffer 1,5mol/L pH 8,8	L20180409-07	Pharmacy of Großhadern Clinic
Tween® 20	9127.2	Carl Roth GmbH + Co. KG

3.1.6 Guides and Template

All guides and the HDR template were designed with Benchling. They were purchased from IDT® (integrated DNA Technologies) and supplied as 25nmol DNA Oligo.

Table 6: Guide sequences

The guide sequences correspond to the CRISPR/Cas9 target sequence in the cell line genome.

		Spacer Sequences	Ref. No.
Mino gRNA	F 1	5‘-CACCGCGAGGAGTAGCTGTGCTACG-3‘	223658393
	R 1	5‘-AAACCGTAGCACAGCTACTCCTCGC-3‘	223658394
Jeko-1 gRNA	F 1	5‘-CACCGGGGGTGTTGTCCACAGGCG-3‘	225290086
	R 1	5‘-AAACCGCCTGTGGACAACACCCCC-3‘	225290087
	F 2	5‘-CACCGCACAGCTACTCCTCGCCTG-3‘	225290088
	R 2	5‘-AAACCAGGCGAGGAGTAGCTGTGC-3‘	225290089
	F 3	5‘-CACCGACCAGTGGTCCAGCTCGTC-3‘	225290090
	R 3	5‘-AAACGACGAGCTGGACCACTGGTC-3‘	225290091

Table 7: HDR template sequence

The HDR template sequence corresponds to the NOTCH1 wildtype sequence, except of two changes. The first change prevented the HDR template of being cut by the CRISPR/Cas9 construct. The other change induced a restriction site for the restriction enzyme SalI.

HDR Template	5’-GCACACTATTCTGCCCCAGGAGAGCCCCGCCCTGCCCACGTCG CTGCCATCCTCGCTGGTCCCACCCGTGACCGCAGCCCAGTTCC TGACGCCCCC**T**TCGCAGCACAGCTACTCCTCGCCTGT**C**GACAA CACCCCCAGCCACCAGCTACAGGTGCCTGAGCACCCCTTCCTC ACCCCGTCCCCTGAGTCCCCTGACCAGT-3’

3.1.7 Antibodies

Antibodies were stored at -20 °C until dilution. After dilution, they were kept up to 3 weeks at 4°C and reused for at most 3 times.

Table 8: Antibodies

	Brand	Dilution
Cleaved Notch 1 (4147S)	Cell Signaling Technology®	1/500 (5% BSA)
Anti-Rabbit IgG, HRP Conjugate (REF W4018)	Promega W4011	1/5000 (5% milk)

3.1.8 Primers

Primers were purchased from metabion international AG and stored at 4°C.

Table 9: Primers

Name	Sequence	Order No.	PO-No.
hU6F 100µM solution	5'-GAGGGCC-TATTTCCCATGATT-3'	N200319-071 W200319-054	2322002632
Notch1 F1 100µM solution	5'-GCAGGTG-CAGCCACAAAACTTA-3'	N200313-043 W200313-040	2322002632
Notch1 Rev 100µM solution	5'-TAAAAAGGCTCCTCTGGTCGGC-3'	N200313-043 W200313-040	2322002632

3.1.9 Anneal gRNAs

Table 10: Anneal gRNAs

	Concentration	Volume		Producer
gRNA F	100µM	20µL	See section 3.1.6	
gRNA R	100µM	20µL	See section 3.1.6	
NEBuffer 4	10x	5µL	#B7004S, Lot 0307	New England BioLabs® Inc.
H_2O	1x	5µL		

3.1.10 Cloning gRNA into CRISPR/Cas9 backbone

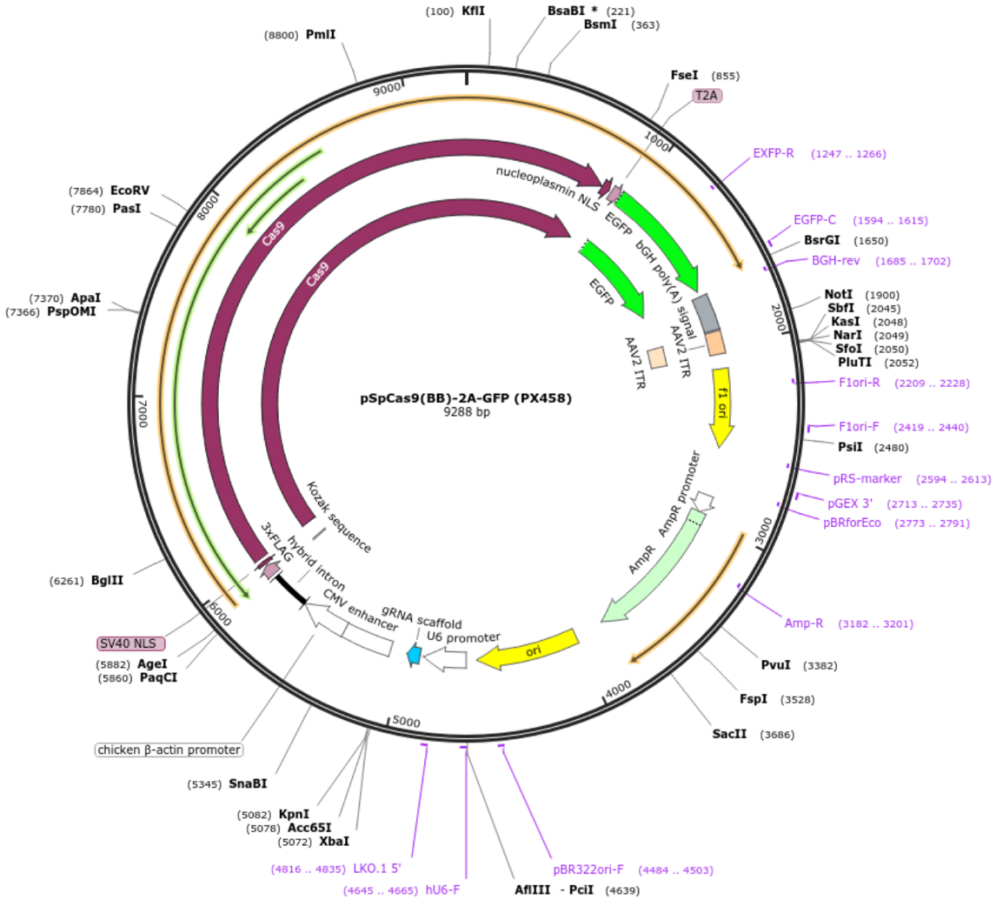

Figure 10: pSpCas 9 backbone PX458 (plasmid, Cat. No 48138), (Addgene homepage)

Feng Zhang Lab, described in Ran et al. The vector size is 9300 bp and has an Ampicillin resistance.

Table 11: Cloning gRNA into backbone

	Cat. No	Producer
pSpCas9 (backbone)	See Figure 10	
Annealed gRNA fragment	See section 3.1.9	
FastDigest Bpil (BbsI)	#FD1014	Thermo Scientific
T4 Ligase, HC (30U/µL)	#EL0014	Thermo Scientific
T4 Ligase Buffer 10x	B69	Thermo Scientific
H_2O	AD	

3.1.11 Commercial kits

Table 12: Commercial kits

	Cat. No.	Producer
AmpliTag Gold® DNA Polymerase with Gold Buffer & $MgCl_2$	REF 4311806	Applied Biosystems by Life Technologies

Annexin V-PE Apoptosis Detection Kit 1	559783	BD Biosciences
EndoFree® Plasmid Maxi Kit	12362	QIAGEN GmbH
MycoAlert™ Mycoplasma Detection Kit (100 Tests)	LT07-318	Lonza
NucleoSpin® Blood QuickPure	REF 740569.250	MACHEREY-NAGEL GmbH & Co. KG
PureLink™ Quick Plasmid Miniprep Kit	REF 210011	Invitrogen™ by life technologies™
QIAquick® PCR purification Kit	28106	QIAGEN GmbH
Quant-iT™ Qubit RNA BR Assaykit	Q10211	ThermoFisher Scientific
Pierce Bovine Serum Albumin Standard Pre-Diluted Set	23208	ThermoFisher Scientific

3.1.12 Western blot gels

Table 13: Western blot gels

Name	Compounds	in mL
5% Stacking Gel for western blot (5mL = 2 gels)	AD 30% acrylamide mix 1,5M Tris-HCl-buffer (pH 6,8) 10% SDS 10% ammonium persulfate TEMED	3,4 0,83 0,63 0,05 0,05 0,005
12% Resolving Gel for western blot (15mL = 2 gels)	AD 30% acrylamide mix 1,5M Tris-HCl-buffer (pH 8,8) 10% SDS 10% ammonium persulfate TEMED	4,9 6,0 3,8 0,15 0,15 0,006

3.1.13 Apparatus

Table 14: Apparatus

Apparatus	Brand
Autoclaves	Systec/Schembera
Bacterial shaker	HT INFORS
Bunsen Brenner	CAMPINGAZ®
Cell culture hood	Trox GmbH
Cell incubator	Binder CO2
Cytospin	Shandon Southern Products Ltd. /Sigma /Thermo/Eppendorf
E-BOX VX5	Vilber Lourmat
FACS Canto II	BD Bioscences
Freezer (-20°C)	Liebherr

Freezer (-80°C)	thermoscientific
Fridge (4°C)	Liebherr
Fusion SL	Vilber Lourmat
GloMax Discover	Promega
Ice machine	Hoshizaki
Magnetic stirrer	Heidolph
Microscope (cell culture)	Motic®
Microscope Dmi8 (fluorescence)	Leica
Multifuge X1R/Megafuge 40R	Heraeus
NanoDrop 1000	PeqLab
Nucleofector 2b	Lonza
peQSTAR 2X Gradient	peQlab
Qubit	ThermoFisher Scientific
Roll mixer	Phoenix Instrument
scale	Kern
Thermo Bloc	HLC
Trans-Blot SD Semi-dry transfer Cell	Bio-Rad Laboratories, Inc.
Vi-Cell XR	Beckman Coulter
Vortex	Scientific Industries

3.1.14 Software

Table 15: Software

Program	Developer
Endnote X9.3.3	Microsoft
Flow Jo, V10	BD Biosciences
Microsoft-Excel for Mac 2020 for Mac V16.66.1	Microsoft
Microsoft-Powerpoint for Mac 2020 V.16.66	Microsoft
Microsoft-Word for Mac 2020 V.16.66.1	Microsoft
Nebiocalculator (mass to mol)	New England Biolabs
TIDE software	Brinkman, E. K., et al. (2014)

3.1.15 Other materials

Table 16: Other materials

Material	Cat. No.	Brand
10mL Stripette®	REF 4488	Corning Incorporated Costar®
14mL Polystyrene Round-Bottom Tub	REF 352051	Falcon® by Corning Science Mexico S.A. de C.V.
2mL Stripette®	REF 4486	Corning Incorporated Costar®
Erlenmeyer narrow-neck flask, capacity 500 mL	Z232831	Duran®
Erlenmeyer wide-neck flask, capacity 250 mL	Z233021	Duran®

5 mL Polystyrene Round-Bottom Tube	REF 352051, Lot 30319041	Falcon® by Corning Science Mexico S.A. de C.V.
5mL Stripette®	REF 4487	Corning Incorporated Costar®
Autoclavable bag, PP	70 01 005	Ratiolab® disposables for science
Cassettes	REF NC2010, Lot 2165710	Novex ® by life technologies™
Cell Culture Microplate, 96 well, PS, U-bottom	REF 650180, Lot E19083LC	Greiner Bio-One GmbH
Cryotube 1,8 mL SI INT, FOOT, ROUND	368632, Lot 165015	Thermo Fisher Scientific
Gel Blot Paper	Cat 10426890, Lot 17084894	GE Healthcare Life Sciences
Gel Loading Tip Round 1-200µL	4853	Costar
Ingenio® 0,2cm Cuvettes	MIR 50121, Lot 02064867	Mirus
Inoculation spreader	REF 86.1569.001, Lot 9083511	SARSTEDT AG & Co. KG
Micro tube 1,5mL SafeSeal	REF 72.706.400	SARSTEDT AG & Co. KG
MILLEX® GP Filter Unit 0,22 µm	REF SLGP033RS, Lot R8PA38136	Merck Millipore Ltd.
NALGENE® Cryo 1°C Freezing Container	5100-0001	NALGENE®
PCR SoftTubes, 0,2mL	711008	Biozym Scientific GmbH
Petri Dish	REF 633180, Lot F1909396/00993	Greiner Bio-One GmbH
Pipette, 25 mL, graduated 2/10mL, sterile, paper-plastic packaging, single packed	REF 760180	Greiner Bio-One GmbH
Research® plus Pipettes PVDF Blotting Membrane	Z683892 10600023	Eppendorf® GE Healthcare Life Sciences Whatman™
Qubit® assay tubes	Q32856	ThermoFisher Scientific
Safe-Lock Tube 2.0 mL	0030120094	Eppendorf AG
Safe-Lock Tubes 0,5mL	0030121023	Eppendorf AG
Solution Basin, 55mL, PS, sterile, 50/PK	HEA20521C	Heathrow Scientific®
TC Flask T25, Susp., Vent. Cap	REF 83.3910.502	SARSTEDT AG & Co. KG
TC Flask T75, Suspen., Vent. Cap	REF 83.3911.502	SARSTEDT AG & Co. KG
TC Plate 12 Well, Standard, F	REF 83.3921	SARSTEDT AG & Co. KG
TC Plate 12 Well, Suspension, F	REF 83.3921.500	SARSTEDT AG & Co. KG
TC Plate 24 Well, Suspension, F	REF 83.3922.500	SARSTEDT AG & Co. KG
TC Plate 6 Well, Suspension, F	REF 83.3920.500	SARSTEDT AG & Co. KG

TC Plate 96 Well, Suspension, F	REF 83.3924.500	SARSTEDT AG & Co. KG
Transferpette® S-8 30-300µL	705912	BRAND
Tube 15mL, 120x17 mm, PP	REF 62.554.502	SARSTEDT AG & Co. KG
Tube 50mL, 114x28mm, PP	REF 62.547.254	Corning incorporated Avenida Industrial del Norte S/N
Vasco® Nitril Soft Blue	REF 9201115	B. Braun Melsungen AG
VWR® Disposable Transfer Pipets	REF 612-4518	VWR International bvba

3.2 Methods

The material references as well as the preparation of the various buffers and solutions are described in section 3.1.

3.2.1 Cell Culture

Mino and Jeko-1 cell lines were cultured in Suspension TC Flasks T25 or T75 at 37°C, 5% CO_2 and 95% relative humidity in a cell incubator. For cell culturing, RPMI 1640 with 10% FBS Standard was used. Cell lines were split 3x per week. Fresh cells were thawed every 3 months. TC Flasks were changed every 3 weeks.

Single cell sorted cells in 96-well, U-well Cell Culture Microplates were cultured in IMDM with 20% FBS Standard and 1/100 AntiAnti 100x. After cell growth, cells were conditioned to grow in RPMI with 20 % FBS to allow later culturing in RPMI with 10% FBS.

All work was performed under the sterile cell culture hood. Before use, it was sterilized with UV-light, which was turned off during work. During work, a vertical airflow was switched on to keep the cell culture hood sterile. Material that was introduced under the sterile cell culture hood from unsterile environment was previously disinfected with Ethanol 70% (LAB).

3.2.2 Cell culture media

RPMI 1640 and IMDM were stored in the fridge at 4°C. FBS Standard was stored in the freezer at -20°C and defrosted at 4°C the day before adding to the RPMI 1640 or IMDM. The rest of the FBS Standard was aliquoted in 50mL tubes, refrozen at -20°C and thawed at 4°C the day before use.

3.2.3 LB-Medium

In a sterile 500mL glass bottle, 10g of LB Broth (Lennox) and 500mL of AD were added and mixed with the magnetic stirrer. It was then autoclaved and after cooldown stored in

the fridge at 4°C. Ampicillin was added under sterile conditions at a concentration of 1µL/1mL shortly before use.

3.2.4 LB-Agar

In a sterile 500mL glass bottle, 17,5g of LB-Agar (Lennox) and 500mL of AD were added and mixed with the magnetic stirrer. It was autoclaved and after cooldown Ampicillin was added at a concentration of 1µL/mL under sterile conditions. The following steps were also performed under the sterile cell culture hood. 20mL of autoclaved LB-Agar were added in a Petri Dish and the Petri Dishes were openly drying for 30min. Then, the plates were closed and stored upside down in the fridge at 4°C until further use.

3.2.5 Freezing cells

$5x10^6$ cultured cells were spun down with 2000rpm for 5min and the supernatant was removed. Under the sterile cell culture hood, the cell pellet was resuspended with 1mL FBS containing 8% DMSO and filled in a Cryotube. The tubes were stored in an Isopropanol-freezing container which allowed the cells to cool down slowly at -80°C for 2h. Afterwards, the samples were stored at -80°C for at least 24h. For long-term storage, the cells were transferred into liquid nitrogen.

3.2.6 Thawing cells

Frozen cells were put in water bath at 37°C until completely thawed. They were then spun down at 2000rpm for 5min and the supernatant was removed. The cell pellet was resuspended in 1mL prewarmed RPMI 1640 with 10% FBS Standard and cultivated the cell incubator as described in section 3.2.1. Cell viability was determined with the Vi-Cell device before each splitting process. Cells were only used for experiments if the viability exceeded 96%.

3.2.7 Trypan blue Cell counting with Vi-Cell XR:

Trypan blue is a deep blue, polyanionic dye used to stain dead cells or tissue. It stains the destroyed membrane of dead cells blue, while it doesn't stain the membrane of living cells.

For the Vi-Cell measurements, 0,6-1 mL of the sample was absorbed by the Vi-Cell device and mixed 1:1 with trypan blue. The sample could be diluted for cell counting and the dilution factor was adapted as needed. The Vi-Cell device took pictures of the stained sample and determined the cell count and viability.

3.2.8 Detection of Mycoplasma contamination

Reagent and Substrate were brought to room temperature. $1x10^6$ cultured cells were spun down for 5min at 1500rpm and 25µL of the supernatant were transferred into a white-bottom 96-well plate. 25µL of the Reagent were added to the sample and incubated for

5min in the GloMax device. The samples were then measured with “1 second integrated reading” (A). 25µL of Substrate were added to the sample and incubated for 10min inside the GloMax. The samples were again measured with “1 second integrated reading” (B). Cells were not infected with mycoplasma if B/A < 1.

3.2.9 Design gRNA for plasmid

Guides were designed with Benchling. In both cell lines, guides targeting the PEST domain in the *NOTCH1* gene were selected. For the Jeko-1, 3 promising pairs that could be able to induce a random mutation in the PEST domain of the *NOTCH1* were selected by the best ON-/OFF-Target score with the algorithms established by Doench et al. (135). For the Mino, 1 pair of guides was selected, targeting the point mutation mentioned in section 3.1.1 in the PEST domain of the *NOTCH1* gene. The chosen sequences are listed in Table 6.

3.2.10 Design HDR template

The HDR template for repairing the PEST domain in the Mino cell line was created on Benchling. It was a 200bp long sequence that corresponded to the wildtype sequence of the PEST domain of the *NOTCH1* gene. Two nucleotide changes that didn’t change the amino acid sequence of the Notch1-protein were introduced for different aims. These changes are shown in Table 7. The first change prevented the HDR template of being cut by the M1 vector. The other change induced a restriction site for the restriction enzyme SalI. This restriction site is essential for checking if the repairing of the *NOTCH1* gene was random or influenced by our HDR template.

3.2.11 Introducing gRNAs into the plasmid

The following steps were inspired by “Protocol for rapid and versatile genome engineering using the MIN (Multifunctional Integrase) Strategy, 1. Using CRISPR/Cas to insert the MIN-tag”(136).

First, the gRNA pairs were annealed by mixing the corresponding gRNAs, the NEBuffer 4 and the water as indicated in section 3.1.9. The mixture was placed in the heating block for 5min at 95°C. Afterwards, the mixture was slowly cooled down to room temperature by switching off the heating block.

The annealed guides were then introduced in the pSpCas9 backbone (plasmid). The reaction mixtures (Mix 1 and Mix 2) were prepared as represented in Table 17. The quantities of the plasmid and annealed gRNA fragments were converted into volumes with help of the Nebiocalculator. The concentration of double-stranded gRNA fragments was measured with the Qubit device as described in section 3.2.14.

Table 17: reaction mixtures (Mix 1 and Mix 2) for introducing the annealed Mino guides into the pSpCas9 backbone

	Mix 1	Mix 2	Positive control	Negative control	pUC19 control
pSpCas9 (backbone)	40fmol	40fmol	40fmol	40fmol	1µL
Annealed gRNA fragment	120fmol	240fmol	/	120fmol	/
Fast Digest BpiI	1µL	1µL	/	1µL	/
T4 Ligase (30U)	1µL	1µL	/	/	/
T4 Ligase Buffer	2µL	2µL	/		/
H_2O	X µL (final volume of sample: 20µL)				/

The reaction mixtures were incubated with the following thermal cycle:

Temperature	Time	Cycle
37°C	5min	55x
20°C	5min	
37°C	60min	1x
65°C	10min	1x

After termination of the thermal cycle, 1µL of FastDigest BpiI was added and the reaction mixtures were incubated for another hour at 37°C. The vectors were then ready to be transformed into E. coli.

3.2.12 Transformation of vectors into E. coli

The following steps were performed under sterile conditions.

Before starting, the Petri dishes with Ampicillin-rich LB-Agar were put at 37°C in the bacterial incubator to preheat. The heating bloc was preheated at 42°C.

The protocol to "transform competent cells" from the product information sheet from Invitrogen was performed.

To check the rightfulness of the vector, it had to be multiplied. Therefore, it had to be transformed into chemically resistant E. coli bacteria. First 50µl of E. coli were thawed on ice and split equally into two 1,5mL Micro tubes. 5µL of the reaction mixtures described in Table 17 containing the vectors were added to the bacteria and the tubes were flicked lightly. For the pUC19 control, 1µL (10pg) of the pUC19 control vector were added to 25µL of the bacteria. The tubes were flicked and put for 30 min on ice. Afterwards, they were put in the preheated heating bloc for 30s, before they were put again on ice for 2min. 500µL of S.O.C. medium was added to the E. coli and they were shaken in the bacterial shaker for 1 hour at 260rpm and 37°C. On one plate, 100µL of the E. coli

mixture were spread on the Ampicillin-rich LB-Agar, and 400 µL were spread on a second plate. The plates were then incubated overnight at 37°C in the bacterial incubator. For the pUC19 control, 100µL and 25µL were spread on the Ampicillin-rich LB-Agar.

The next day, grown colonies were picked with a sterile pipette tip and each grown in 2mL sterile LB-Medium with 1µL/mL Ampicillin in the bacterial shaker at 37°C for 4-6 hours in 14mL Polystyrene Round Bottom Tubes. 500µL were used for a Quick Plasmid Miniprep, following the protocol included in the kit. The other 1,5mL were frozen for further use as described in section 3.2.13.

3.2.13 Freeze transformed bacteria

The following steps were done under sterile conditions. The transformed bacteria in LB-Medium were mixed 50:50 with sterile glycerol 60%. 1mL was transferred in a Cryotube. The bacteria were frozen at -80°C.

3.2.14 Quantification of double-stranded gRNA

Double-stranded gRNA was quantified with the Qubit® device. To prepare the Qubit® working solution, Qubit® dsDNA BR Reagent was diluted 1:200 in Qubit® dsDNA BR Buffer. For the standards, 190µL of working solution was required, whereas per sample 198µL were needed. The 2 standards (Qubit® dsDNA BR Standard #1 and Qubit® dsDNA BR Standard #2) were prepared by adding 10µL of one standard to 190µL of working solution and mixed by vortexing for 2-3 seconds. The standards were incubated for 2min before calibrating the Qubit device. On the device, the "RNA Broad Range Assay"-option was selected. The samples were prepared by adding 2µL of the double-stranded gRNA sample to 198µL of working solution. The mixture was vortexed for 2-3 seconds and incubated for 2 minutes before being measured with the Qubit device. The Qubit device automatically calculated the concentration of the original gRNA sample.

3.2.15 Quantification of DNA

Plasmid DNA, double-stranded DNA and purified PCR products were quantified with the Nanodrop device. The device was calibrated with 1,5µL H_2O. 1,5µL of the buffer/the water used to dilute or elute the DNA or PCR sample were used to define a blank. Afterwards, 1,5µL of the samples were measured.

3.2.16 Sequencing (GATC)

Plasmid DNA and purified PCR products were sequenced by GATC. Plasmid DNA was diluted with AD at 80-100ng/µL, the PCR products between 300-1000bp were concentrated at 12ng/µL. 5µL of the diluted DNA sample were added to 5µL of corresponding primer (5µM). The 10µL mixture was send in a 1,5mL Micro tube to GATC where a LIGHTRUN was performed. The sequencing results were retrieved from the Eurofins Genomics website.

3.2.17 Multiplication of plasmids

The following steps were performed under sterile conditions. The surface of the frozen transformed bacteria was scratched with a sterile pipette tip. The pipette tip was added to 2mL prewarmed, Ampicillin-rich LB-Medium in a 14mL Polystyrene Round Bottom Tube and incubated in the bacterial shaker at 260rpm and 37°C for 4-6h. A negative control with a sterile pipette tip was done to check if the LB-medium was not getting contaminated during this process. After incubation, 500µL of the mixture were added to 100mL LB medium in a 500mL Erlenmeyer flask. This mixture was incubated overnight at 260prm and 37°C in the bacterial shaker. The plasmid was isolated from the bacteria with the Quick-Start Protocol from EndoFree® Plasmid Maxi Kit. The plasmid was sequenced with GATC to check if the annealed gRNAs had been successfully introduced into the pSpCas9 backbone. The sample was prepared as mentioned in section 3.2.16.

3.2.18 Transfections

Transfections were performed as electroporation under the sterile cell culture hood. 30min before beginning, 1,5mL of RPMI 1640 with 20% FBS per sample was prewarmed in a 12-well suspension plate in the cell incubator. $2x10^6$ cells (Mino or Jeko-1) were centrifuged in a 2mL Safe-Lock Tube for 90xg for 10min. The supernatant was removed by careful pipetting. The cell pellet was resuspended cautiously with 100µL Ingenio® Solution. Afterwards, one or more vectors (pSpCas9 backbone, M1, J1, J2 and/or J3) were added, as well as the HDR template for the Mino cells. The mixture was transferred to an Ingenio® 0,2cm Cuvette and a chosen program was applicated on the Nucleofector 2b device. 500µL of the previously prewarmed RPMI 1640 medium were added to the cuvette and the cells were rested for 30s-1min before being transferred to the prewarmed RPMI 1640 medium in the suspension 12-well plate. For a better cell survival, it is important that all steps after addition of the Ingenio® Solution were performed as rapidly and carefully as possible. The 12-well plate containing the transfected cells was incubated for 48h before measuring the samples with the FACS as described in section 3.2.20 or for 24h before single cell sorting as described in section 3.2.22.

3.2.19 Electroporation Optimization

To optimize the electroporation process, different programs from the Lonza protocol "Amaxa® Cell Line Optimization Nucleofector® Kit" were performed on the cell lines Mino and Jeko-1 with the pSpCas9 backbone. To determine the most promising program, 2µg of the pmaxGFP™ vector was used. After choosing the best program, vector quantity had to be optimized. Different vector quantities as shown in Table 27 were used.

A negative control without any vector was performed with every preparation.

3.2.20 FACS GFP measurement

To determine the effectiveness of the transfection optimization with different transfection programs or vector concentrations, the transfected Mino and Jeko-1 cells were measured with the FACS device for GFP positivity. The pSpCas9 vector contains a *GFP* gene and therefore successfully transfected cells fluorescence green. To prepare samples for FACS

measurement, 500µL of the transfected cells were spun down 5min at 2000rpm in a 5 mL Polystyrene Round-Bottom Tube. The supernatant was tilted and 300µL PBS were added. 5µL of Propidium Iodide Solution (50µg/mL) were added shortly before the FACS measurements to stain dead cells. The sample was vortexed before being measured with the FACS device. The sample was screened for PI and GFP, and the voltages were adapted to each cell line as necessary.

3.2.21 Microscope fluorescent-positive cells (GFP)

The following steps were performed under sterile conditions in the cell culture hood. In order to prepare the transfected cells for a look under the fluorescence microscope, 500µL of the cells were centrifuged at 2000rpm for 5min. The supernatant was tilted. The cell pellet was resuspended with 300µL of PBS and transferred to a 24-well plate. Under a 10x optical enlargement, the fluorescence light was activated, and the GFP-positive cells could be observed.

To retake the cells in culture, the cells were transferred from the 24-well plate in an Eppendorf tube and centrifuged for 5min at 2000rpm. The supernatant was removed, and the cell pellet was resuspended with 500µL of RPMI 1640 and taken into culture.

3.2.22 Single cell sorting

For single cell sorting, cells had to be tested negative for Mycoplasma as described in section 3.2.8.

The following steps were all performed under sterile conditions in the cell culture hood.

In order to create good single cell sort conditions, single cells had to be sorted into prewarmed medium. Therefore, the day before sorting, 96-well, U-well plates were prepared and prewarmed in the cell culture incubator overnight. With a multichannel pipette, 100µL IMDM with 20% FBS Standard and 1/100 AntiAnti were added to the wells.

The transfection was performed as described in section 3.2.18 and cells were incubated for 24h in 12-well plates.

Before sorting, the transfected Mino and Jeko-1 cells were centrifuged at 300xg for 5min, and the supernatant was removed. The cell pellet was washed once with FACS solution. Afterwards, 1mL of FACS solution was added to the cell pellet. 3 different samples were prepared as shown in Table 18. Sample 1 simply contained electroporated cells without the vector. Sample 2 contained the same cells as sample 1, but 5µL of Propidium Iodide Solution (PI) was added. Sample 3 contained the cells transfected with the vector, that were also stained with 5µL op PI. The samples were stored on ice until they were single sorted on GFP-positivity with the FACS. After the single cell sort, the cells were incubated at 37°C, 5%CO_2 and 95% humidity. The single cell sort was kindly performed in the Labor für Leukämiediagnostik of the Klinikum der Universität München – Großhadern, Medizinische Klinik III by their technical staff. Dead cells were stained using PI. PI negative cells were analyzed on their GFP positivity and the GFP positive cells were single cell sorted into a 96-well, U-well plate and incubated at 37°C in the cell incubator for the next weeks. Potential cell growth was controlled on a regular basis every three days under the microscope.

Table 18: The 3 different preparations for cell sorting

Sample No.	GFP	PI
1 (PI - control)	(-)	(-)
2 (PI + control)	(-)	(+)
3 (transfected)	(+)	(+)

3.2.23 Polymerase chain reaction (PCR)

The PCR was performed with isolated DNA from cell lines. The PCR reaction mixture was prepared as described in Table 19.

Table 19: PCR reaction mixture

Reagents	Volume (µL)
DNA (100ng/µL)	1
primer Notch1 F1	1
primer Notch 1 Rev	1
10x ATG buffer	2,5
dNTP's (2,5mM)	2,5
$MgCl_2$ (25mM)	2,5
DMSO	1,25
AmpliTag Gold®	0,3
H_2O	12,95
Total	**25**

The DNA fragments were amplified using the following heating cycle:

Time	No. of cycles	Temperature
2min	1x	95°C
30s	3x (for each temperature)	94°C
40s		74/70/66/62/58°C
1min		68°C
30s	20x	94°C
40s		54°C
1min		68°C
5min	1x	68°C

20 µL of the reaction mixture containing the amplified DNA fragments were purified with the QIAquick® PCR purification Kit and prepared for sequencing as described in section 3.2.16. The other 5µL were used for Agarose gel electrophoresis as mentioned in section 3.2.24.

3.2.24 Agarose gel electrophoresis

Agarose gel electrophoresis was used to determine the length of the DNA fragments obtained in the PCR. First, an Agarose 1% gel was prepared by mixing 1g of Agarose NEEO ultra-quality with 100mL of 1x TAE buffer. This preparation was microwaved until the Agarose powder was completely diluted. 10µL of SYBR® Safe DNA Gel Stain were added, and the preparation was poured into a cast. To be able to later load samples in the gel, a comb was added immediately in order to create wells in the gel. Then, the gel was dried for 1h.

The DNA fragments were prepared by adding 1µL of Loading Dye to 5µL of the sample or DNA ladder. Afterwards, the comb was removed from the dried gels, 1x TAE buffer was added to the Electrophoresis chamber until the gel was completely submerged and the samples were loaded into the wells. An electric current of 121V was applied for 45min.

DNA fragments were visualized with UV-light in the E-BOX VX5 device.

3.2.25 DLL4 stimulation

The DLL4 stimulation of the cell lines Mino and Jeko-1 was performed under sterile conditions.

In a 12-well, adherent plate, 500µL of PBS with 4µg/mL DLL4 was added. The plate was centrifuged at 300xg for 5min before being incubated for 4h at 4°C. 1mL of $0{,}5x10^6$ cells/mL were added to the wells, and the plates were centrifuged at 300xg for 5min. The plates were incubated for 48h in the cell culture incubator at 37°C, 5% CO_2 and 95% humidity.

3.2.26 Protein extraction

The method for protein extraction was performed as described in the protocol for Lysis of Mammalian Cells in Suspension (Cat. No. 04719956001) from Roche. The working solution was slightly adapted by adding 1µL of each Phosphatase Inhibitor Cocktail 2 and 3 per 10.000 cells.

3.2.27 Bradford Assay (Protein Quantification)

After protein extraction from cells, protein quantification was essential before running a western blot

Bio-Rad Protein Assay Dye Reagent Concentrate was diluted 1/5 with AD. Each Bradford Assay Standard and protein lysate sample was prepared and measured in doublets.

In a 96-well plate, 200µL of the diluted Protein Assay Dye Reagent were added to each well. 5µL of Protein Standards, Protein Lysis Buffer or Protein Sample were added into the wells as samples. The absorbances were measured with the GloMax device. Protein concentrations were deduced from a standard curve determined by the absorbance of the Protein Standards.

3.2.28 Western blot

Western blot gels were prepared 1-7 days before running the Western blot. The different components were mixed as mentioned in Table 13. After adding APS and TEMED to the Resolving Gel, the mixture was vortexed and put immediately into Western Blot Cassettes. Isopropanol 70% was added on top of the Resolving Gel and was let set for 30 min. Afterwards, the Isopropanol was discarded, and the Stacking Gel is added into the Cassette. A 10-compartment comb was inserted carefully in the Stacking Gel and was let set for 30min. Afterwards, the cassettes were put in the fridge at 4°C under humid conditions.

The gels were loaded with up to 20µg protein using a maximum of 23µL per compartment, and 5µL of peqGOLD Protein V (ladder).

The Western blot was run with 61V for 30min, 81V for 90min and 121V for 60min. It could be stopped earlier if the protein had already run through.

3.2.29 Transfer Western blot gel to membrane

The blotting membrane was activated in methanol. The methanol was washed off with AD. The blotting membrane was stored in gel-transfer-buffer until used. The gel blot paper was soaked in gel-transfer-buffer, before three layers of gel-blot-paper were added to the Trans-Blot device. First, the activated blotting membrane and then the Western blot gels were put on top of the gel blot paper. Three layers of gel blot paper and more gel-transfer-buffer were added, and the Trans-blot device was closed. The transfer process was performed with 250mA for 2h30. The voltage had to strictly stay under 25V.

After the run, the blotting membranes were put in 50mL tubes and the proteins were blocked in 10mL milk 5% for 1h to prevent later added antibodies from unspecific binding to the membrane. Afterwards, the membranes were washed 3x in 3mL TBST before adding the primary antibody.

3.2.30 Antibodies and detection of antibodies

Used antibodies are listed in Table 20. 2mL of diluted primary antibody were added to the blotting membranes and incubated overnight at 4°C. The primary antibody was tilted and the membranes were washed 3x with TBST for 10min. The diluted secondary antibody was added, and the tubes were incubated at room temperature for 1 hour. Afterwards, the membranes were washed 3x with TBST for 10min.

Table 20: Antibodies for protein detection

Target	Brand	Dilution	Role
Cleaved Notch1 (Val 1744)	Cell Signaling Technology®	1/500 (5% BSA)	Primary antibody
Anti-Actin Antibody	Sigma Aldrich	1/5000 (G-NET)	Primary antibody
Anti-Rabbit	Promega W4011	1/5000 (5% milk)	Secondary antibody

For the detection of the antibodies, detection solution A (SA), detection solution B (SB) and H_2O_2 were mixed in a light-protected 10mL Falcon tube. The blotting membranes were incubated in the dark for 2-5min in the solution mixture. The mixture was then washed off with AD. The membranes were put in the Fusion device and exposed for 10min for the cleaved Notch1 antibody and 3min for the Actin antibody.

4 Results

4.1 CRISPR/Cas9 - Successful annealing and cloning of gRNAs

The objective of this study was to induce a change in the PEST domain of the *NOTCH1* gene of Mino and Jeko-1 cells. Therefore, a CRISPR/Cas9 construct targeting this specific site in the genome of these cells was created. The bacterial pSpCas9 plasmid PX458 shown in Figure 10 was used as backbone of this construct. It served as a vector for carrying specific gRNA into the cells. The gRNA corresponded to the specific site in the genome of the Mino and Jeko-1 cells, which the CRISPR/Cas9 construct targeted to induce a DSB. Before introducing the gRNA into the pSpCas9 backbone, the forward and reverse gRNA strand had to be annealed.

The annealing process was performed as described in section 3.2.11. To verify the correct annealing of the forward and the reverse gRNA of each pair to create the corresponding vectors M1, J1, J2 and J3, the amount of double-stranded gRNA was measured with the Qubit device. Successful annealing resulted in the possibility of double-stranded gRNA detection. The concentration of double-stranded DNA per sample is shown in Table 21. It was used for the calculation of the required amount of the gRNA sample needed for introducing the annealed guides into the pSpCas9 backbone (plasmid).

Table 21: double- stranded gRNA concentrations for the corresponding vectors (M1, J1, J2 and J3) after annealing of gRNA pairs

gRNA for corresponding vector	Concentration (ng/µL)
M1	412
J1	480
J2	557
J3	450

To transform the concentration into moles, the Nebiocalculator was used. The cloning of the annealed gRNAs into the plasmid was successfully performed as described in section 3.2.11.

4.2 Transformation of the CRISPR/Cas9 construct into E. coli

After introducing the annealed gRNA into the pSpCas9 backbone, the CRISPR/Cas9 construct had to be transformed into E.coli in order to be produced by the bacteria. To establish the optimal conditions for the transformation process as described in section 3.2.12 , the M1 plasmid was used. In the case of a successful transformation of the CRISPR/Cas9 construct into E. coli, it obtained an Ampicillin resistance. E. coli containing the CRISPR/Cas9 construct could therefore be grown in an Ampicillin rich environment (LB-Agar and LB-Medium with Ampicillin) in contrast to unsuccessfully transformed bacteria.

As represented by Table 22, the vector M1 generated by Mix 1 was successfully introduced into E. coli. The construct from Mix 2 could not be transformed into E. coli, as no growth on the Ampicillin-rich LB-Agar could be observed. The positive control as well as the pUC19 control also showed a growth of colonies. In the Petri Dish of the negative control, no growth of bacterial colonies was observed, which confirmed that the transformation process was performed under sterile conditions.

Table 22: number of grown colonies containing the M1 plasmid

	400µL spread	100µL spread	25µL spread
Mix 1	1 (M1C1)	1 (M1C2)	/
Mix 2	0	0	/
Positive control	3 (M1C3-5)	/	/
Negative control	0	/	/
pUC19 control	/	13	2

The transformed E. coli with Mix 1 showed grown colonies, whereas the E.coli transformed with Mix 2 didn't show any. Therefore, the vector M1 obtained from Mix 1 was considered as the most effective for the transformation into E. coli. As a result, for the introduction of the annealed gRNAs J1, J2 and J3 into the pSpCas9 backbone, the proportions of Mix 1 were used. The resulting vectors J1, J2 and J3 had also been successfully transformed into E. coli.

4.3 Verification of the vector using Miniprep

The successfully transformed, Ampicillin-resistant E. coli were cultivated in Ampicillin-rich LB-medium in order to multiply the vectors M1, J1, J2 and J3. The vectors were isolated from E. coli with the PureLink™ Quick Plasmid Miniprep Kit and sent to GATC for sequencing. By sequencing, the successful introduction of the annealed guides was proven. As shown in Table 23, the forward sequence of the gRNAs M1, J1, J2 and J3 were found in the area of the pSpCas9 backbone targeted by the BpiI restriction enzyme. The bacterial colonies showing the cleanest sequence (M1Co1T1, J1Co1T1, J2Co1T1, J3Co1T1) were frozen and stored at -80°C as described in section 3.2.13 and used for the following Maxiprep.

Table 23: Miniprep plasmid DNA sequences for the vectors M1, J1, J2 and J3 from different colonies (Co) and takes (T)

The gRNA sequence in the CRISPR/Cas9 construct targeting the NOTCH1 gene is written in bold. Changes to the wildtype CRISPR/Cas9 construct or the gRNA sequence are written in red. In disrupted sequences, no clear DNA sequence was identified.

vector	colony	take	Sequence (5´- 3´)
M1	Co1	T1	AAGGACGAAA**CACCGCGAGGAGTAGCTGTGCTACG**GTTTTAGAGC
		T2	AAGGACGAAA**CACCGCGAGGAGTAGCTGTGCTACG**GTTTTAGAGC
	Co2	T1	AAGGACAAAA**CACCGCGAGGAGTAGCTGTGCTACG**GTTTTAGAGC
		T2	disrupted sequence
J1	Co1	T1	AAGGACGAAA**CACCGGGGGTGTTGTCCACAGGCG**GTTTTAGAGC
		T2	AAGGACGAAA**CACCGGGGGTGTTGTCCACAGGCG**GTTTTAGAGC
	Co2	T1	AAGGACGAAA**CACCGGGGGTGTTGTCCACAGGCG**GTTTTAGAGC
		T2	disrupted sequence
J2	Co1	T1	AAGGACGAAA**CACCGCACAGCTACTCCTCGCCTG**GTTTTAGAGC
		T2	AAGGACGAAA**CACCGCACAGCTACTCCTCGCCTG**GTTTTAGAGC

J3	Co1	T1	AAGGACGAAA**CACCGACCAGTGGTCCAGCTCGTC**GTTTTAGAGC
		T2	AAGGACGAAA**CACCGACCAGTGGTCCAGCTCGTC**GTTTTAGAGC
	Co2	T1	AAGGACGAAA**CACCGACCAGTGGTCCAGCTCGTC**GTTTTAGAGC
		T2	AAGGACGAAA**CACCGACCAGTGGTCCAGCTCGTC**GTTTTAGAGC
	Co3	T1	AAGGACGAAA**CACCGACCAGTGGTCCAGCTCGTC**GTTTTAGAGC
		T2	disrupted sequence

4.4 Verification of the vector using Maxiprep

For the transfection of the vectors M1, J1, J2 and J3 into Mino and Jeko-1 cells, larger quantities of the plasmids were required. The chosen bacterial colonies from section 4.3 were multiplied as described in section 3.2.17 and isolated from E. coli with the Quick-Start Protocol from EndoFree® Plasmid Maxi Kit. As shown in Table 24, the forward sequence of the respective gRNAs M1, J1, J2 and J3 could be found in the area of the pSpCas9 backbone targeted by the Bpil restriction enzyme. These isolated vectors were further used to perform the transfections with the mammalian cell lines Mino and Jeko-1.

Table 24: Maxiprep plasmid DNA sequences for the vectors M1, J1, J2 and J3.

The introduced gRNA sequence in the CRISPR/Cas9 construct targeting the NOTCH1 gene is written in bold. All the sequences corresponded to the gRNA sequences.

vector	Sequence (5´-3´)
M1	AAGGACGAAA**CACCGCGAGGAGTAGCTGTGCTACG**GTTTTAGAGC
J1	AAGGACGAAA**CACCGGGGGTGTTGTCCACAGGCG**GTTTTAGAGC
J2	AAGGACGAAA**CACCGCACAGCTACTCCTCGCCTG**GTTTTAGAGC
J3	AAGGACGAAA**CACCGACCAGTGGTCCAGCTCGTC**GTTTTAGAGC

4.5 Optimization of the electroporation process

The next step was to transfect the plasmids M1, J1, J2 and J3 into cell lines Mino and Jeko-1. The electroporation process was very critical and had to be specifically optimized for each of the two cell lines as discussed in section 5.2 and 5.3 . The optimal transfection program and vector quantity is a combination of a good cell survival as well as a considerable GFP positivity in the surviving cells. Too high voltage or pulse time, or too much vector quantity would have damaged the cells and ended in cell death. A program too weak or a vector quantity too low results in the vector not being able to get into the cells and therefore in a lack of GFP positivity as a sign of an unsuccessful transfection.

Transfections were performed as described in section 3.2.18.

The first step consisted of transfecting the pSpCas9 backbone into the cell lines Mino and Jeko-1. Table 25 shows the survival rate of the transfected cells, and the percentage of GFP positive cells in the surviving population. The Mino cell line was very sensitive. To the electroporation process. Cell survival was very low, except for the program A-020. As the results didn't look promising, the Lonza Scientific Support Team advised to further try the transfection programs A-030, D-016 and T-013 for the Mino cell line with the pmaxGFP^{TM} vector. For the Jeko-1 cell line, it was decided to try further transfections with the programs X-001 and L-029, as they showed an acceptable cell survival rate as

well as a GFP positivity (Table 25). The program A-020 also showed a good survival of the Jeko-1 cells, but seemed too weak, because no GFP positivity was observed.

Table 25: Cell survival and GFP positivity (GFP+) after transfection of the pSpCas9 backbone (2µg) into the mammalian cell lines Mino and Jeko-1

For transfection with the pSpCas9 backbone, program A-020 from the proposed Lonza optimization programs looked most promising in the Mino cell line. To get even better results, the Lonza Scientific Support Team advised further transfections with the programs A-030, D-016 and T-013 with the Mino cells. For the Jeko-1 cell line, it was advised to try further experiences with X-001 and L-029.

Mino				**Jeko-1**		
Program	**Population (%)**			**Program**	**Population (%)**	
A-020	Survival	32,7		A-020	Survival	37,2
	GFP+	3,91			GFP+	0
T-020	Survival	0,63		T-020	Survival	2,34
	GFP+	0			GFP+	0
T-030	Survival	0,25		T-030	Survival	0,51
	GFP+	0			GFP+	0
X-001	Survival	6,91		X-001	Survival	25,3
	GFP+	2,26			GFP+	0,099
X-005	Survival	2,32		X-005	Survival	13,7
	GFP+	2,99			GFP+	0,13
L-029	Survival	1,15		L-029	Survival	20,1
	GFP+	0			GFP+	0,28
D-023	Survival	2,46		D-023	Survival	12,6
	GFP+	0			GFP+	0,12
M-013	Survival	1,59		M-013	Survival	29,5
	GFP+	4,17			GFP+	0,18

The next step for optimizing the transfection process for the Mino and Jeko-1 cell lines consisted in transfecting 2µg of the pmaxGFP™ vector. The pmaxGFP™ vector is a plasmid which is used in order to establish the most effective transfection program for each cell line. The samples were analyzed with the FACS Canto II device as described in section 3.2.20 and the results deduced with the Flow Jo software are showed in Table 26.

Table 26: Cell survival and GFP positivity after transfection of the pmaxGFP™ vector (2µg) into the mammalian cell lines Mino and Jeko-1

The transfection optimization was proceeded with the pmaxGFP™ vector and the programs advised by the Lonza Scientific Support Team. For the Mino cell line, program A-030 showed a good survival and GFP positivity. For the Jeko-1 cells, the program X-001 showed an acceptable survival and a lot of GFP positivity.

Mino				**Jeko-1**		
Program	**Population (%)**			**Program**	**Population (%)**	
A-020	Survival	87,8		X-001	Survival	51,5
	GFP+	8,37			GFP+	70,1
D-016	Survival	62,4		L-029	Survival	44,9
	GFP+	7,19			GFP+	44,6

A-030	Survival	74	
	GFP+	42,7	
T-013	Survival	18,8	
	GFP+	4,05	

To visualize the results obtained by the FACS measurements, the samples were also observed under the fluorescence microscope. The images are shown in Figure 11.

Mino cells showed a good survival rate for all the programs except T-013, which was considered too strong. Program A-030 showed by far the best GFP positivity in the FACS analysis. A strong GFP positivity after application of the program A-030 had also been observed under the fluorescence microscope. Program A-030 was therefore used in all further transfection optimizing processes with the Mino cell line.

Jeko-1 cells showed an acceptable survival for both programs X-001 and L-029. As cell survival and GFP positivity was a little higher with program X-001, this program was chosen for further optimization of the transfection process with different vector quantities.

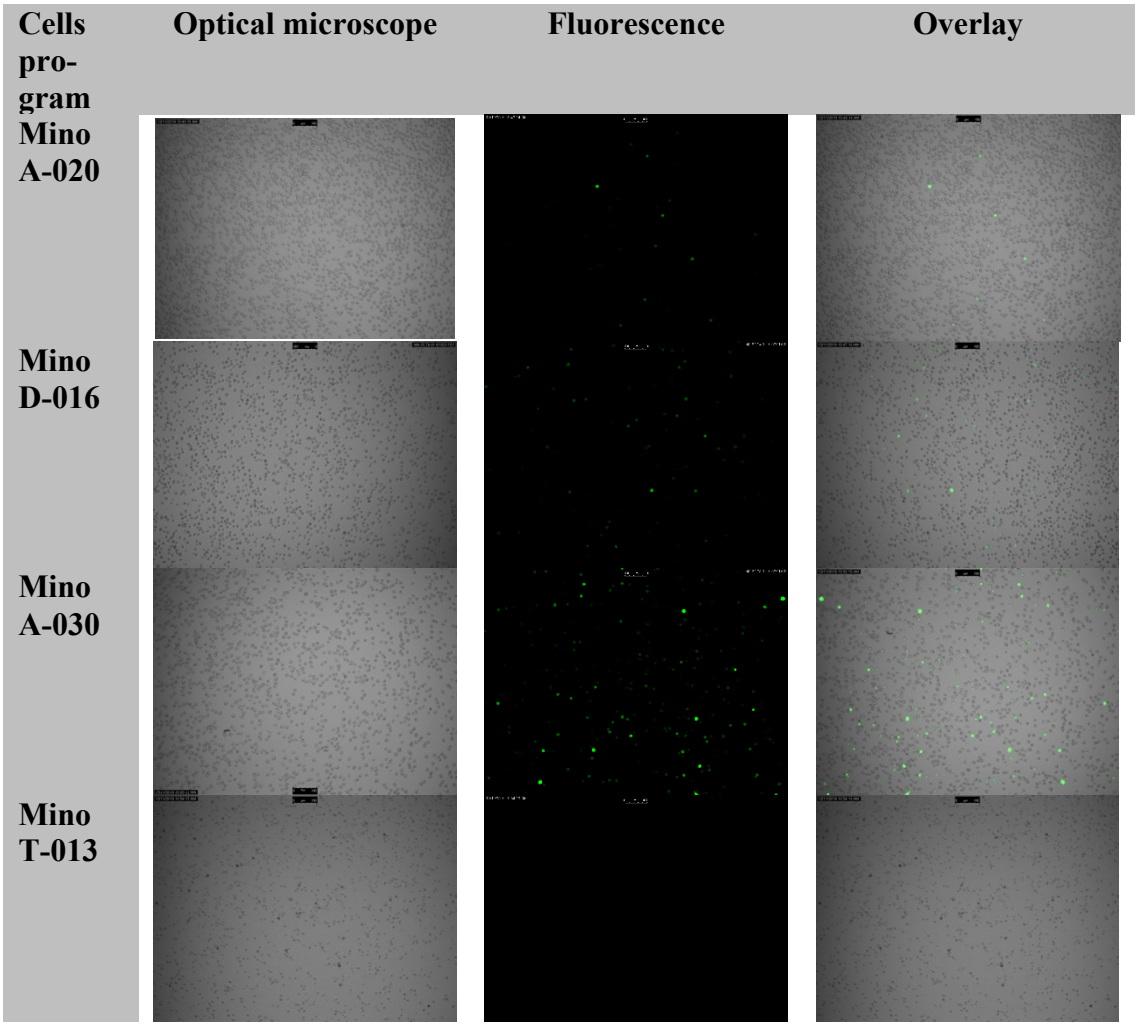

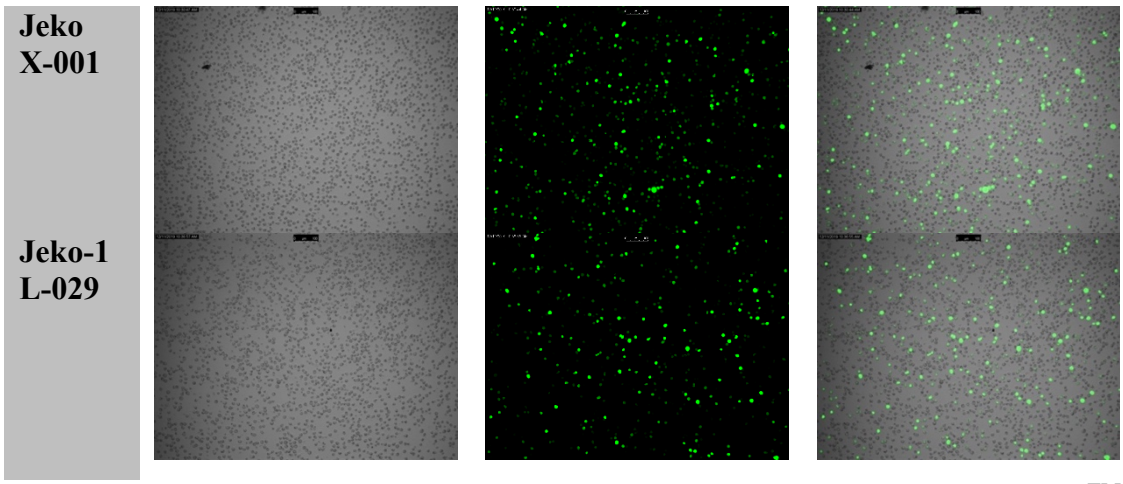

Figure 11: Fluorescence microscopy images after transfection of the pmaxGFP™ vector (2µg) into the mammalian cell lines Mino and Jeko-1

The last step of the transfection optimization process was the adaption of the vector quantity. For this step, the vectors M1 for the Mino cell line and the vector J1 for the Jeko-1 cell line were used. As shown in Table 27, first, a broad range of different vector quantities was tested. Based on these results, more specific vector quantities were tested. For the Mino cell line, the most effective transfection was done with the transfection program A-030 and 14µg of the corresponding vector M1. For the Jeko-1 cell line, the first vector quantities were too elevated. As higher vector quantities induced a reduced cell survival, the vector quantity of 4µg was chosen and used with the transfection program X-001 for optimal transfection results.

Table 27: Cell survival and GFP positivity for different vector M1 and J1 quantities

First, a broad spectrum of vector concentrations was applied in the cell transfection process (left column). After defining the best range of concentrations, more specific concentrations were applied (right column).

Mino – Program A-030 – Vector M1					
Vector quantity (µg)	**Population (%)**		**Vector quantity (µg)**	**Population (%)**	
6	Survival	48,1	10	Survival	56,4
	GFP+	1,0		GFP+	0,44
9	Survival	35,1	11	Survival	48,7
	GFP+	1,1		GFP+	1,34
12	Survival	26,6	12	Survival	40,1
	GFP+	2,3		GFP+	1,84
15	Survival	28,7	13	Survival	52,3
	GFP+	1,0		GFP+	1,33
			14	Survival	42,8
				GFP+	2,07
			15	Survival	38,2
				GFP+	1,42

Jeko-1 – Program X-001 – Vector J1					
Vector quantity (µg)	**Population (%)**		**Vector quantity (µg)**	**Population (%)**	
6	Survival	8,77	3	Survival	41,7
	GFP+	0,24		GFP+	0,04
9	Survival	7,64	4	Survival	12,2
	GFP+	0,03		GFP+	0,24
12	Survival	6,3	5	Survival	20,6
	GFP+	0,24		GFP+	0,15
15	Survival	7,6	6	Survival	15,9
	GFP+	0		GFP+	1,31

4.6 Single cell sort and growth of the Mino cell line

The Mino cells were prepared for the single cell sort as described in section 3.2.22. The statistics of the Mino cell sort are shown in Figure 12. Even though the Mino cells revealed an acceptable survival rate and GFP positivity rate after transfection with the vector M1 and the HDR template in FACS analysis, no cell growth was observed in the 96-well plates.

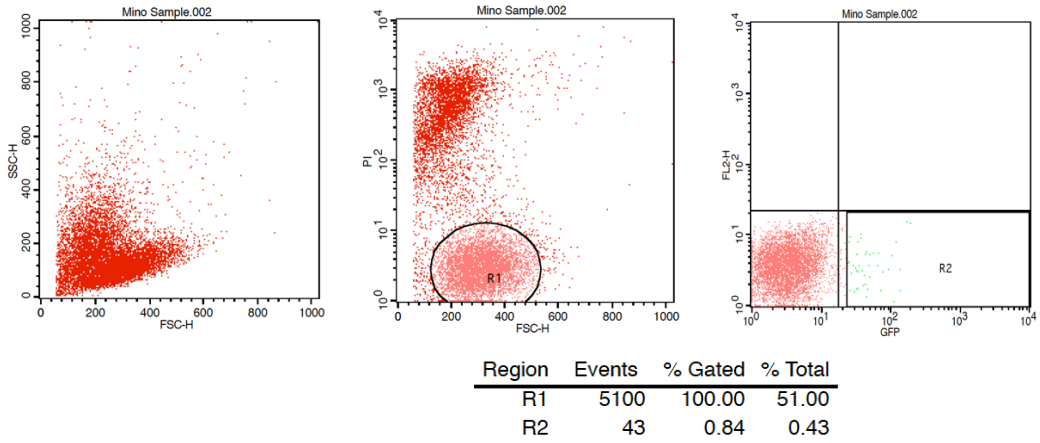

Figure 12: Statistics of the Mino single cell sort

The single cell sorts were kindly performed by the technical assistant from the Labor für Leukämiediagnostik of the Klinikum der Universität München – Großhadern, Medizinische Klinik III, as representative for other single cell sorts.

After unsuccessful Mino cell growth, we next controlled if the Mino cell line was able to grow after the transfection and single cell sort process. Therefore, 3 different Mino populations were used. The untreated Mino cells (U) were native Mino cells that were not transfected and directly sorted from an incubated cell culture sample. Mino Control cells (C) were treated with the previously established transfection program A-030, but without the M1 vector or HDR template. Mino GFP cells (GFP) were transfected with the transfection program A-030 and 14µg of the M1 vector and 2,47µg of the HDR template. Additionally, as RPMI 1640 20%, the standard medium for Mino cells, flocked out in previous single cell sorts, IMDM was also tested. The results are shown in Table 28.

None of the Mino GFP cells showed any cell growth in either of the media. For the Mino Control cells, there was no growth in RPMI 1640 20% medium, but an important cell growth in the IMDM 20% medium had been observed. The untreated, single sorted Mino cells showed a growth in both media. This approach showed that the use of IMDM medium was by far the most effective and should be used for further single cell sorts. In RPMI 1640 20% medium, a flocculation of the FBS after 1 week was observed which probably interfered with cell growth.

Table 28: Number of colonies grown from single cell sort with untreated Mino cells (U), Mino Control cells (C) and Mino Transfected with the GFP positive vector M1 (GFP) and in different cell culture medium (IMDM and RPMI 1640)

Medium	sample	Number of 96-well plates	Week 2	Week 3	Week 4
IMDM 20% FBS	Mino U	2	19	23	21
	Mino C	2	14	17	16
	Mino GFP	1	0	0	0
RPMI 1640 20% FBS	Mino U	2	0	1	2
	Mino C	2	0	0	0
	Mino GFP	4	0	0	0

4.7 Single cell sort and growth of the Jeko-1 cell line

The Jeko-1 cells were prepared and stained for single cell sort similar to the Mino cells as described in section 3.2.22. For each vector J1, J2, J3 and their different combinations, a separate sample was prepared. The results of the Jeko-1 single cell sort are shown in Table 29. Jeko-1 cells revealed a low to acceptable survival and a low GFP positivity rate after transfection with the vectors J1, J2, J3 and their different combinations. Overall, there were enough GFP positive cells that were sorted into 1-2 96-well U-bottom plates filled with IMDM 20% FBS medium.

Table 29: Region statistics of the Jeko-1 single cell sort

Vector	Region	Events	% Gated	% Total
J1	PI-	1714	100	17,14
	GFP +	2	0,12	0,02
J2	PI-	4561	100	45,61
	GFP +	7	0,15	0,07
J3	PI-	4732	100	47,32
	GFP +	5	0,11	0,05
J1+2	PI-	5003	100	50,03
	GFP +	12	0,24	0,12
J1+3	PI-	4996	100	49,96
	GFP +	6	0,12	0,06
J2+3	PI-	5933	100	59,33
	GFP +	5	0,08	0,05
J1+2+3	PI-	6662	100	66,62
	GFP +	8	0,12	0,08

First signs of cell growth of the single cell clones were observed 1-2 weeks after the cell sorting. In the following days, more and more clones grew. An overview of colony growth

is represented in Table 30. The thriving clones were expanded into larger wells as soon as the cell colonies became visible on a macroscopic level. The expanding was continued until the colonies were cultivated in 6-well suspension plates.

Table 30: Jeko-1 cell growth of transfected Jeko-1 cells with different vectors (J1, J2, J3 and combinations) after single cell sort

The number of macroscopically visible Jeko-1 clone populations in the 96- well plates was counted after 14 and 24 days. If after 24 days, the clone population was not visible on a macroscopic level, cell growth was considered as unsuccessful for that clone.

vector	After 14 days	After 24 days
J1	4	4
J2	4	6
J3	6	6
J1+2	14	18
J1+3	5	5
J2+3	5	5
J1+2+3	6	6

The next step was checking if a random mutation that disabled the PEST domain of the *NOTCH1* gene had occurred. To look for promising clones, DNA was isolated from the Jeko-1 clones and sequenced by GATC in order to look for a disruption in the PEST domain of the *NOTCH1* gene in these clones.

4.8 Sequencing of Jeko-1 clones

After transfecting the Jeko-1 cells with the corresponding vectors, a DSB leading to a modification downwards the target area is expected. This should be noticeable in the target region of the CRISPR/Cas9 construct, as a mixed nucleotide sequence or the presence of indels should be observable by target sequencing.

In the GATC DNA sequences, most of the clones (Figure 13B) showed a clean wildtype sequence of the PEST domain of the *NOTCH1* gene. In these clones, the *NOTCH1* gene was probably not disrupted (Figure 13B), and wildtype Notch1 protein levels were observed by western blot (section 4.10). Other clones (Figure 13A) showed a disruption in the region where the vectors J1, J2 and J3 targeted the *NOTCH1* gene. Here, the CRISPR/Cas9 construct had likely induced a double strand break, which was afterwards repaired by NHEJ. At this point, Jeko-1 clones could only be separated in wildtype or modified clones. These modified clones were classified as promising clones. To determine the effectiveness of the modification, further analysis was needed. For the vectors J1, J2 and the different combinations of the 3 vectors, at least one promising Jeko-1 clone was found. The transfection of vector J3 resulted only in wildtype clones.

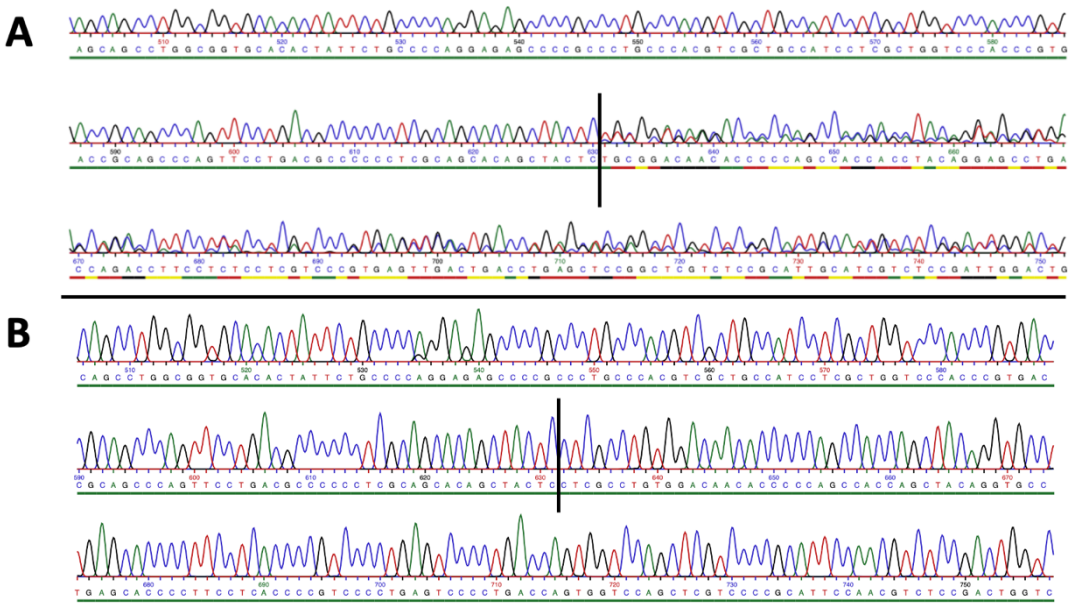

Figure 13: wildtype and mutated *NOTCH1* gene sequences in Jeko-1 clones after treatment with the CRISPR/Cas9 J1 vector, sequenced by GATC.

A: *This sequence shows a promising Jeko-1 clone after treatment with the J1 vector. In the beginning, the sequence is clean without background noise. This changes after the target point of the J1 vector determined by the gRNA (see section 3.2.9).*
B: *This sequence shows a Jeko-1 clone after treatment with J1 vector without an induced change. The sequence corresponds to the Jeko-1 wildtype sequence and shows no background noise even after the target point of the J1 vector.*

The promising clones were then analyzed with the TIDE software as representatively shown with the Jeko-1 J1 clone in Figure 14. The quality control confirmed that the sequence of the J1 clone changed after the expected CRISPR/Cas9 targeted break site. The overall efficiency allows to determine which fraction of PCR product contained mutations. In the bar graph, the indel occurrences in the changed sequences are compared. The statistically relevant indels in the case of the J1 clones are -2, -1 and +1 indels and would result in frameshift mutations.

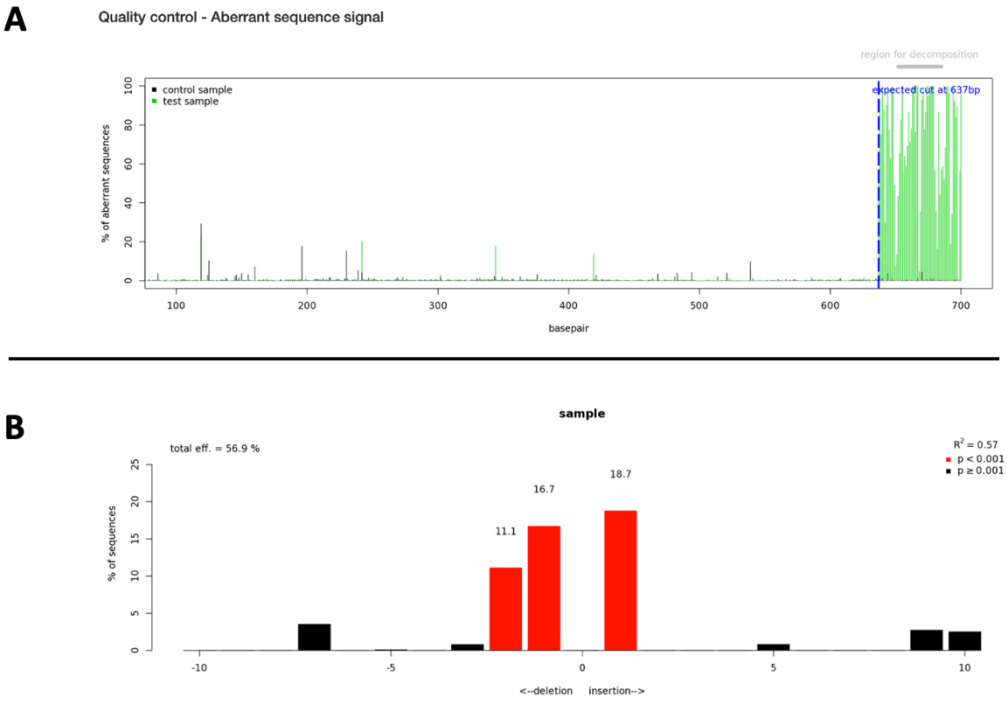

Figure 14: TIDE software analysis of the Jeko-1 clone sequence after treatment with the J1 vector in comparison to the wildtype *NOTCH1* sequence (Brinkman et al., 2014) (137)

A: *This figure shows the sequence of Jeko-1 clone after treatment with the J1 vector in comparison to the wildtype NOTCH1 sequence. The control sample (black) shows a low and equally distributed signal, the Jeko-1 clone (green) shows a low signal before the break site (blue line) and an expected increased signal downstream of the expected cut.*
B: *The CRISPR/Cas 9 induced insertions and deletions are determined by the TIDE software. As representation the Jeko-1 clone after treatment with the J1 vector is shown. 56,9% of the sequences in the PCR mix contain an induced mutation, statistically relevant indels (red) are insertions of +1 nucleotide or deletions of -1 or -2 nucleotides. Statistics for the other Jeko-1 clones are resumed in Table 31.*

Table 31: Statistics of the TIDE software analysis of sequences of the Jeko-1 clones after treatment with the different CRISPR/Cas9 vectors and their combinations in comparison to the wildtype NOTCH1 sequence

Jeko-1 clone	Total Efficiency	Deletion	Insertion
J1	56,90%	**-1**: 16,7%; **-2** 11,1 %	**+1**: 18,7%
J2	53,70%	**-1**: 14,2 %	**+1**: 22,5%
J1+2	44,60%	**-5**: 29,5	/
J1+3	37,80%	**-2**: 7,9%	**+1**: 9,3%
J2+3	21,30%	**0**: 45,3%	
J1+2+3	26,80%	/	**+6**: 6,7%

4.9 Agarose gel electrophoresis

After sequencing the Jeko-1 clones, the clones with disrupted sequences after the vector target were analyzed by agarose gel electrophoresis. With this method, the length of a chosen sequence can be compared to see if an insertion or a deletion have happened. In

this case, the CRISPR/Cas9 targeted region of PEST domain in the *NOTCH1* gene was amplified by PCR as described in section 3.2.23 for agarose gel electrophoresis.

The DNA from the Jeko-1 clones for PCR was isolated at two time points: the first DNA isolation was done as soon as there were enough cells grown from the single cell colonies, the second isolation was done one month after the first one in order to verify gene stability. Results are shown in Figure 15. The Jeko-1 and Mino control DNA had the same length, as they differed just by a point mutation. The DNA fragments of the Jeko-1 clones did not show large differences in length, but were mostly shorter than the wildtype fragment. This implicates that the modifications in the Jeko-1 clones are deletions. The J1 clone shows a broad brand, which could mean that heterozygote modifications resulting in two different gene lengths could have been introduced.

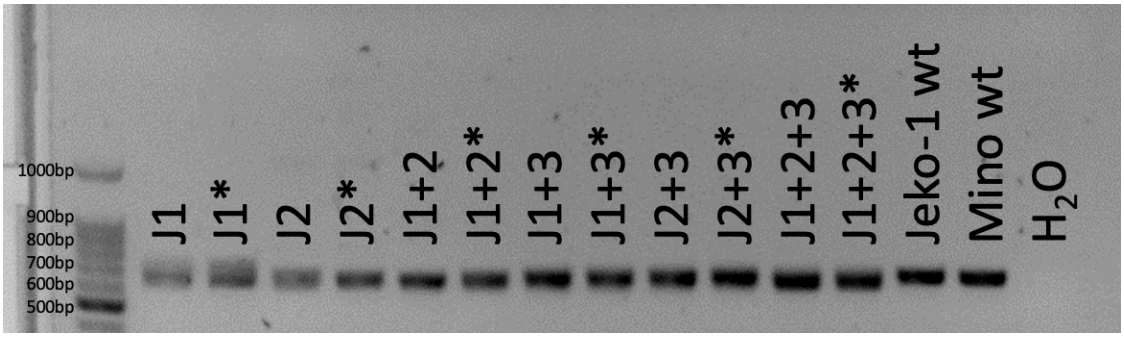

Figure 15: Agarose gel electrophoresis of the PEST domain of the *NOTCH1* gene with the F1 primer of the Jeko-1 clones in the beginning and after one month (*) in comparison to the Jeko-1 and Mino wildtype (wt)

4.10 Verification of the effectiveness of the introduced modifications

In order to verify the effectiveness of the introduced modifications on the protein level, the Notch1 protein had to be stimulated by DLL4 as described in section 3.2.25. As showed in Figure 16, DLL4-stimulation of the Mino cells, harboring a *NOTCH1* mutation in the PEST domain, resulted in overexpression of cleaved Notch1 protein, whereas in unmutated Jeko-1 cells, Notch1 protein expression was not visible in the western blot analysis even if the Jeko-1 cells were stimulated.

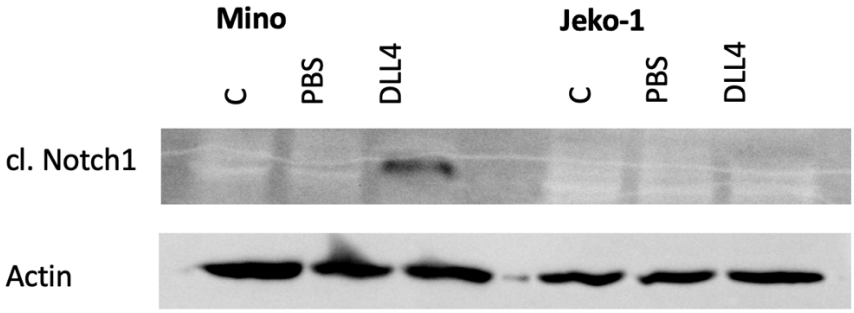

Figure 16: cleaved Notch1 protein in DLL4 stimulated and unstimulated Mino and Jeko-1 wildtype cells

With this method, we next analyzed if mutations in the DNA sequences of the Jeko-1 clones lead to a dysfunctional, more stable protein. For every vector and their combination, except for J3, one promising Jeko-1 clone was stimulated with DLL4 as described in section 3.2.25. The cleaved Notch1 protein of the DLL4 stimulated Jeko-1 cells was used as negative control whereas the cleaved Notch1 protein of the DLL4 stimulated Mino cells was used as positive control.

As shown in Figure 17, western blot analysis revealed that all of the clones evaluated expressed a dysfunctional Notch1 protein with increased protein expression of cleaved Notch1. The protein length of the cleaved Notch1 protein was shorter than the wildtype cleaved Notch1 protein for J1, J2 and J1+2, whereas J2+3 and J1+2+3 presented a longer sequence than the wildtype Notch1 protein. The J1+3 clone shows two protein bands. As expected, the Mino protein was around 10kDa shorter than the wildtype Notch1 protein because of the preliminary stop codon.

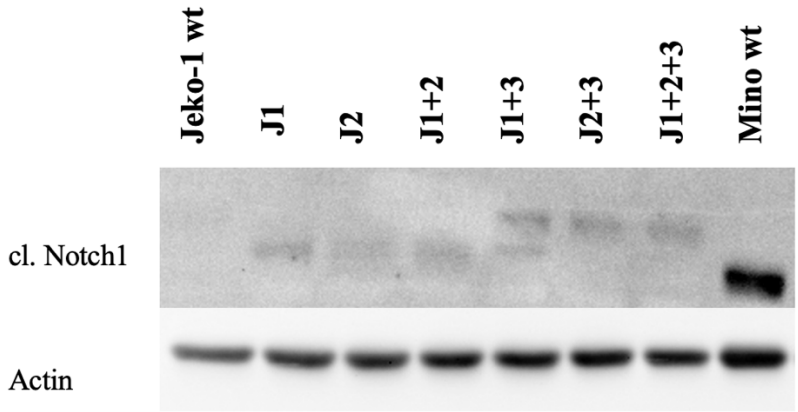

Figure 17: cleaved Notch1 protein (cl. Notch1) in DLL4 stimulated Jeko-1 clones in comparison to DLL4 stimulated Jeko-1 and Mino wildtype (wt)

5 Discussion

5.1 *NOTCH1* gene mutations as a potential therapy target in MCL

Mantle Cell Lymphoma is an aggressive subtype of Non-Hodgkin Lymphoma. The primary oncogenic event is the translocation t(11;14)(q13;q32) resulting in Cyclin D1 overexpression. Other driver mutations are *TP53*, *ATM* and *MLL2(22, 23)*. Furthermore, multiple studies detected recurrent *NOTCH1* mutations in MCL and their negative prognostic effect and defined their use as potential therapeutical target (22, 42, 75, 77).

Inhibition of Notch1 activity can occur through disruption of the Notch1 signaling pathway. A potential approach is the use of γ-secretase inhibitors (GSI) or monoclonal antibodies (mAb). γ-secretase inhibitors (GSIs) already show good results in preclinical studies in T-ALL and CLL but can only be used in low-dosed combination therapies because of their severe side effects when used in high-dosed monotherapy. (86-88). Disappointingly, McCaw TR et al. showed that GSI have no clinical benefit in most solid tumors (138). Further research is indispensable to fully understand the clinical potential of GSI in MCL therapy. Simultaneously, more specific *NOTCH1* targeting therapies have to be developed. In this regard, Anti-Notch1 antibodies are assessed. Xie et al. showed promising *in vivo* effects of OMP-52M51 (Brontictuzumab) in adenoid cystic carcinoma of the trachea (139). OMP-52M51 (Brontictuzumab) or MAb604.107 are currently probed in T-ALL (90, 91, 140).

In this study, CRISPR/Cas9-mediated gene editing was performed to modify the PEST domain of the *NOTCH1* gene in the cell lines Mino and Jeko-1 aiming to characterize specific effects of *NOTCH1* mutations without interference of intercellular differences. Genetic heterogeneity, epigenetic patterns and microenvironmental factors can influence the effect of therapeutic substances (141). Che et al. already successfully used CRISPR/Cas9 editing to analyze the effect of *PRMT* to DNA damage-repairing capacity and to validate the target efficiency of PRMT5 inhibitors by generating MCL cell line Granta-519, Maver-1 and Z-138 knockout clones (142).

5.2 The CRISPR/Cas9 method as an efficient gene editor in MCL

The CRISPR/Cas9 method is a new and efficient molecular biology method to introduce modifications into the genome of a cell. As mentioned in section 1.3.3, this method is already tested widely in the medical field (115-122).

The preparation of a CRISPR/Cas9 construct targeting a specific region in the genome is resumed in Figure 18. The construct targets a specific region determined by the gRNA and creates a double strand break, which is then mostly repaired by NHEJ, or more rarely by HDR if an HDR template is available (109). As described in section 1.3.2, NHEJ is error-prone, and therefore, random modifications in form of insertions or deletions can take place. In this study, the CRISPR/Cas9 method was used to introduce modifications into MCL cell lines in order to create genetically identical clones just differing by a mutation in the PEST domain of the *NOTCH1* gene.

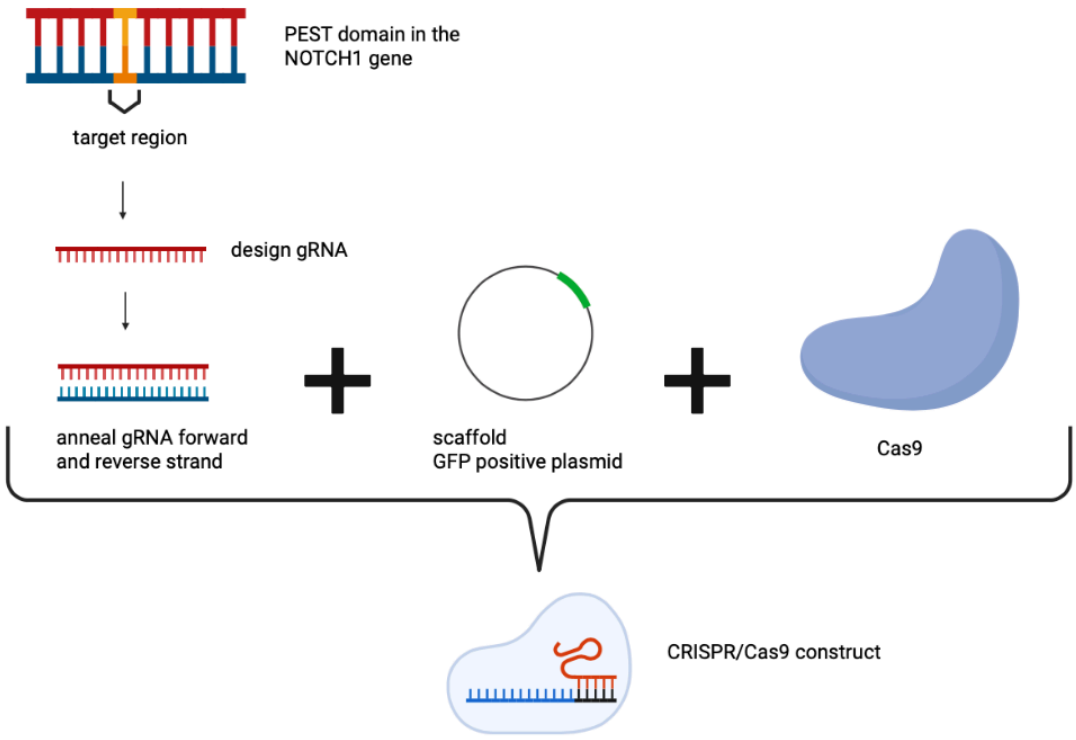

Figure 18: overview of the construction of a CRISPR/Cas9 construct

The guide RNA was designed with Benchling and selected by the best ON-/OFF-Target score with the algorithms established by Doench et al. (135). The ON-Target score describes the probability of the CRISPR/Cas9 vector to target a specific site, the OFF-Target score indicates the probability of undesired hits. The predictions are calculated by algorithms, but it is controversial how these predictions agree with the actual measurements and on which specific factors they depend (143-145). For the construction of the vector, every construction step could be verified. Potential problems would have been detected after each step.

In the Mino cell line, the objective of this study was to repair the point mutation described in section 3.1.1 to get a wildtype sequence *NOTCH1* gene. Primarily, a CRISPR/Cas9-mediated double strand break was induced. Moreover, for HDR reparation, a donor template was additionally needed. Different forms of HDR templates exist single-stranded donor oligonucleotides, double-stranded plasmid DNA donors or adeno-associated viruses (146, 147). The single-stranded DNA is commonly used for smaller modifications as it is the most effective, whereas plasmid DNA is used for large insertions such as entire proteins. In this study, a single stranded donor template was used. A weakness of this system is that it could not be controlled if the HDR template actually entered the cells with electroporation. The GFP positive cells containing the vector did not necessarily contain the HDR template. Kunwoo et al. showed that it is less effective to transfect the CRISPR/Cas9 construct independently from the HDR template than to complex the gRNA with the HDR template. This ensures that single cell sorted cells do not only contain the CRISPR/Cas9 construct, but also the HDR template (148).

As HDR is less efficient as NHEJ, the HDR process should be optimized. Small molecule inhibitors are studied to inhibit NHEJ or enhance HDR (149, 150). Yu et al. tested nearly 4000 small molecules to identify two promising candidates for HDR enhancement (151) In addition, Nambiar et al. suggest that a modification of RAD18, a protein involved in

post-replication repair pathways, may improve the efficiency of CRISPR/Cas9-mediated HDR repair (152).

Moreover, the transfection process was a critical point in this study. Figure 18 gives an overview of the electroporation process. The detailed description of the process is noted in section 3.2.18.

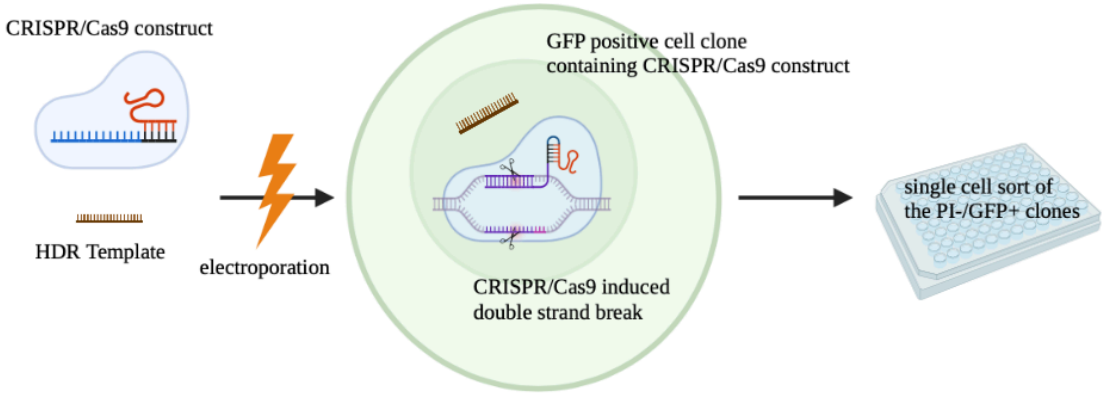

Figure 19: Electroporation of the CRISPR/Cas9 construct into the MCL cells Mino and Jeko-1.

As stated in section 2.1.1, the Mino and Jeko-1 cell lines were established MCL cell lines, with a constant mutated or wildtype NOTCH1 gene. The transfection of the cell lines with the CRISPR/Cas9 vector and the HDR template was performed by electroporation. Fus-Kujawa et al. state that the optimal transfection method takes different factors into account such as transfection efficacy and cell toxicity. Moreover, it should be adapted on the experimental design and objective (153). The electroporation process has the advantage that it is more efficient than other transfection options such as chemical transfection. Moreover, it requires lower DNA quantity. Although, a major problem of the technique is that it potentially results in high cell damage (154). Cells have to be treated carefully during the transfection steps to reduce further cell death.

In this study, for each of the cell lines Mino and Jeko-1, an efficient electroporation program was established. Electroporation optimization primarily depended on the optimal program. Jordan et al. states that factors as the electroporation waveform, the voltage and the pulse duration play an important role (155). The Nucleofector 2b used in this study did not allow to adjust these parameters independently, as the device had predefined programs. A predetermined list of orientating transfection programs had to be performed and afterwards, a few promising programs were suggested by the Lonza Scientific Support Team. The cell survival after transfection did not only depend on the programs, but also on the execution of the experiment. As also described in other studies, the state of the cells before transfection and performing the transfection steps quickly while pipetting cautiously were crucial (156).

After the first few single cell sorts of the transfected cells in 96 U-bottom wells with the standard RPMI 20% FBS medium, both Mino and Jeko-1 clones showed low survival. Even with adding FBS to the cell sorting buffer, perturbations of metabolic stress during single cell sorting cannot be prevented (157). A potential reason for low cell survival was linked to a precipitate formed in the bottom of the wells. It led to an impossibility for clones to grow in the 96-well plates. Reasons for medium precipitation could be the relation of small volume correlated to the surface of the 96-well plate and therefore high

evaporation and concentration of the medium components or a contamination (158). Under the microscope, contamination was not detected. The previously described problem was optimized by the use of IMDM medium, another standard medium used in cell culture. In other single cell sort studies, Dulbecco´s modified Eagle Medium (DMEM) achieved a good cell growth for single cell sorting (159). In this study, IMDM showed acceptable stability and did not flock in the 96-well plates, allowing cell growth from the single cell sort. Munoz et al. underline the importance of optimized cloning medium for ensuring single-cell survival (159).

Table 32: differences in composition of RPMI 1640 and IMDM retrieved from the pan-biotech.de website

	RPMI 1640	**IMDM**
Glutamine	L-glutamine	stable glutamine
HEPES	-	+
Phosphate	++	+
Calcium	Calcium nitrate	Calcium chloride anhydrous

Table 32 shows some of the differences in medium composition of RPMI 1640 medium and IMDM. Stable glutamine, contained in IMDM, is more stable than L-glutamine, which can spontaneously break down to form ammonia and therefore can damage cells. The toxicity of ammonia in cell culture medium is a common problem (160). Therefore, products such as GlutaMax, a stable glutamine, are indispensable (161, 162). HEPES is a buffer, efficient in the pH range 6,8-8,2, which stabilizes the medium (163, 164). pH destabilization could result in cell death. Soluble calcium forms are contained in both media. Calcium nitrate in the RPMI medium could have possibly been no longer soluble and as a consequence, flocking out (165). This could destabilize the cell culture medium and also end in cell death. By using IMDM in the 96-well plates for single cell sort, formation of precipitates no longer occurred and transfected cells could grow up from a single cell sort.

Taken together, transfection programs for the Nucleofector 2b could be established for both cell lines. For the Mino cell lines, the best results were achieved with the transfection program A-030, whereas the Jeko-1 cell line was transfected with the program X-001. Careful handling of the samples while performing the transfection process was essential and could influence cell survival significantly. Moreover, IMDM medium in the 96-well plates showed a huge benefit for single cell sorting in comparison to RPMI medium. Altogether, the CRISPR/Cas9 method is an important tool in medical research. It allows precise genome editing at reasonable cost (166). Unfortunately, the method also has its weak points, such as the unquantifiable OFF-target effect and the double strand break associated p53-toxicity.

5.3 Insights on CRISPR/Cas9 editing in Mino and Jeko-1 cells

In the Mino cells, the clones died after transfection with the CRISPR/Cas9 construct and the HDR template. To date, there is no data on transfection or CRISPR/Cas9 editing in the Mino cell line. Additionally, no data on single cell sorting of Mino cells is available. In our study, FACS analysis showed that the CRISPR/Cas 9 construct M1 entered the cells through transfection, as they showed GFP positivity. Nevertheless, after the single cell sort, there were no Mino clones growing. To identify potential disruptive factors,

different preparations (untreated, control and transfected) of Mino cells as described in section 4.6 were single cell sorted and the results shown in Table 28. It showed that Mino clones could potentially grow in a single cell sort, even after application of the transfection program A-030. The disruption in the Mino clones must therefore be related to the M1 construct and the HDR template. The preparations were also performed in the two different media RPMI and IMDM. RPMI medium was flocking out and creating a toxic environment with low cell growth in any assay as discussed in 5.2. For IMDM, there was Mino cell growth for the untreated and control cells, but not for the transfected cells. This shows on one hand that for the Mino cell line, it is possible to grow from single cell sort without further measures, and on the other hand that the cell line survives the application of the transfection program A-030. Therefore, the problem was probably related to the introduced CRISPR/Cas9 construct.

There are many possible reasons for CRISPR/Cas9 induced cell death. An important OFF-target effect, a Notch1 dependency of the Mino cells or an overload of introduced DNA in form of the M1 vector and the template are some examples (167). To reduce OFF-target effect, a CRISPR/Cas9 construct with another gRNA targeting the same region could be tried (168). Another potential solution for cell survival could be the use of CRISPR/Cas9 base editors. In comparison to the CRISPR/Cas9 method used in this study, base editors have the advantage that they introduce point mutations in a specific site, without introduction of a HDR donor template and without causing a double strand break (169). This reduces cell damage and optimizes cell survival. A disadvantage of this method is that it also has a considerable OFF-target effect (170). To further reduce OFF-target effects, engineered Cas9 variants such as high-fidelity CRISPR/Cas9 nucleases for example SpCas9-HF1 are currently developed (171, 172). Concerning a potential *NOTCH1* dependency of the Mino cell line, the influence of *NOTCH1* modulation is yet to be completely understood. In other studies, *NOTCH1* shows to have an anti-apoptotic effect and subsequently the inhibition of NOTCH1 leads to increased apoptosis (173, 174). Jang et al showed that downregulation of *NOTCH1* is able to induce apoptosis in murine erythroleukemia (175). The CRISPR/Cas9-mediated HDR of the point mutation in the Mino cells should lead to a wildtype Notch1 protein that is less stable. It is a possibility that therefore, with the downregulation of the *NOTCH1* expression in the Mino cells, the anti-apoptotic effect is also reduced which could subsequently lead to apoptotic cell death. High concentrations of introduced DNA can result in cellular toxicity by inducing cellular stress or activating innate immune responses (176).

Moreover, Álvarez et al. discuss a gene-independent, *TP53* dependent toxicity caused by double-strand breaks (177). Haapaniemi et al. report that CRISPR/Cas9 induced DSB can result in growth arrest associated with p53 (178). An inhibition of p53 could increase the editing efficiency, as CRISPR/Cas9 editing works better in cells without p53 (179). The Mino cell line used in this study overexpresses p53. The transfection with the CRISPR/Cas9 construct in this cell line ended in cell death, which could be explained due to a p53-mediated apoptosis induced by the DSB. On the other hand, in the Jeko-1 cell line, a cell line with *TP53* wildtype, the reparation of CRISPR/Cas9 induced DSB and its repair by NHEJ was successful and Jeko-1 clones grew from single cell sort. The lack of p53 expression can therefore play an important role in effective CRISPR/Cas9 editing.

In Jeko-1 cells, carrier of the wildtype *NOTCH1* gene, the transfection process was successful and Jeko-1 clones were grown from the single cell sort. Promising Jeko-1 clones were defined as presenting sequence changes in the area targeted by the J1, J2 and J3 constructs. These clones had a potentially disruptive *NOTCH1* gene mutation. As the sequences were disrupted as shown in Figure 13, a clear determination of which change had

happened and if the mutation was homozygous or heterozygous was not possible. An agarose gel electrophoresis on a PCR amplification of the targeted DNA sequence and Notch1 protein expression analysis following DLL4 stimulation by western blot were performed. In Figure 15, the agarose gel electrophoresis shows the length of the determined DNA fragment which includes the CRISPR/Cas9 target region. The Jeko-1 wildtype and the Mino fragments were the same length, as they just differ by a point mutation. The Jeko-1 clones showed slightly variating lengths, which could be a sign for potential indels in the analyzed part of the DNA. Successful CRISRP/Cas9 editing in the mantle cell lymphoma cell line Jeko-1 is already described for inducing a deletion in the *ALOX5* gene (180).

After the CRISPR/Cas9 induced double strand break, DNA was mostly repaired by NHEJ, which is error-prone and can lead to deletions, insertions or point mutations (181). The Jeko-1 clone J1 showed a broad band (Figure 13) in the PCR, which could have been a sign for a heterozygous mutation or a mixed clone population. Schneider et al. also demonstrated that CRISPR/Cas9 editing can result in homo- and heterozygous mutations (182). Furthermore, the sequences for each clone were compared to the sequence of the same clone after one month to verify if the genome of clone population was stable. As seen in the agarose gel electrophoresis, the sequence length of the determined DNA fragments stayed the same for every Jeko-1 clone over this period. However, the agarose gel electrophoresis gives no information about the potency of the introduced mutations into the Jeko-1 clones.

The TIDE sequence analysis of the Jeko-1 clones in comparison to the Jeko-1 wildtype cells confirmed that the disruption in the sequence of the Jeko-1 clones corresponded to the expected break site of the CRISPR/Cas9 construct (Figure 14A). The overall efficiency shows the percentage of mutated DNA fragments in the sample. Table 31 represents the statistically relevant indels evaluated by the TIDE software. Most of the indels would be responsible for a frameshift mutation, relocating the stop codon in the *NOTCH1* gene. Considering these results, it cannot be determined if the analyzed cell clone is monoclonal or a mixed population. In order to verify the effectiveness of these mutations on the protein level, DLL4 stimulated Notch1 protein expression was tested for these clones (see section 5.4).

As shown in Figure 17, all promising Jeko-1 clones from section 4.8 with disrupted sequences were probably modified by the CRISPR/Cas9 constructs and carried a potent *NOTCH1* mutation as DLL4 stimulation led to increased expression of cl. Notch1 protein in the western blot analysis. In contrast, the Jeko-1 wildtype cells did not stably express cl. Notch1 protein after DLL4 stimulation. The protein bands of the clones differed by their length, which was presumably either due to the insertion of a premature stop codon for the shorter proteins or a later stop codon for the longer proteins caused by the frameshift of the indels as discussed above. Interestingly, the Jeko-1 J1+3 clone showed two bands in the western blot, indicating that the CRISPR/Cas9 induced change potentially was heterozygous and resulted in two Notch1 proteins of different lengths. Moreover, it is a possibility that the Jeko-1 clone population is a mixed population. Even though single cell sorting has high monoclonality rates, it could be that the sequenced population was not monoclonal (183) . Definitive results can only be obtained by performing next generation sequencing.

In comparison to the Jeko-1 clones, it appeared that the *NOTCH1* gene mutation in the Mino cells is more potent as the Notch1 protein expression level after DLL4 stimulation was higher (Figure 17). Moreover, the Notch1 protein of the Mino cells was significantly

shorter than the Notch1 protein of the Jeko-1 clones, which represents the shortened Notch1 protein by the known preliminary stop codon in the PEST domain of these cells.

5.4 DLL4 as a potent stimulator in *NOTCH1* mutated cell clones

As mentioned in section 1.2.1, Delta-like ligands (DLL1, -3, -4) and Serrate-like ligands (Jagged 1 and 2) are known as *NOTCH1* stimulators. López-Guerra et al. found that the potency of DLL4 for *in vitro* stimulation of the Notch1 pathway in *NOTCH1* mutated CLL cells was the strongest in comparison to the other Notch1 stimulators (184). In *NOTCH1* mutated MCL cells, stimulation with DLL4 lead to increased Notch1 signaling, whereas in Notch1-unmutated MCL cells, no stable overexpression of cleaved Notch1 could be induced by DLL4 (92).

In order to verify the effectiveness of the introduced modifications, cells were stimulated by DLL4 as described in section 3.2.25. As shown in Figure 16, western blot analysis revealed that all of the CRISPR/Cas9 clones evaluated expressed a dysfunctional Notch1 protein with increased protein expression of cleaved Notch1 upon stimulation with DLL4 due to the mutations introduced in the PEST domain.

In conclusion, we successfully managed to create *NOTCH1*-mutated Jeko-1 clones with increased protein expression of cleaved Notch 1, thus delivering the basis for further functional analysis of the biological impact of *NOTCH1* mutations and to evaluate the efficacy of specific Notch1 inhibitors.

5.5 Conclusion and innovations for further studies

NOTCH1 mutations correlate with a negative prognosis in MCL and are an important target for innovative therapies. In this study, a mutation in the PEST domain of the *NOTCH1* gene has been successfully introduced in the Jeko-1 MCL cells using the CRISPR/Cas9 method. In comparison to the Jeko-1 cells with a *NOTCH1* wildtype gene expression, the Jeko-1 mutated clones partially lacked the degradation domain of the *NOTCH1* gene which resulted in an overexpression of cl. Notch1 protein in western blot. However, none of the Jeko-1 clones presented a mutation as potent as the Mino mutation. Tests to show if the induced mutations are functionally relevant need to be performed with survival-, migration- and angiogenesis assays as well as cell cycle and apoptosis analysis. Furthermore, effectiveness of *NOTCH1* targeted therapies should be evaluated by comparing *NOTCH1* mutated and unmutated Jeko1-cells.

The premature cell death of the transfected Mino clones showed that even though CRISPR/Cas9 bears a great potential for experimental and clinical use, it also has its limitations. As discussed in 5.3, the reason for Mino cell death after transfection could not be determined certainly. For further investigation, the transfection of the Mino cells should be repeated with other guides, targeting a different sequence of the Mino DNA. This could change the unpredictable OFF-target effect and cells could potentially survive. Mino cells could also be transfected with and without the HDR template, to see if the reason for cell death may be a DNA overload. Another option would be to inhibit p53 prior to the transfection in order to reduce p53-assosciated toxicity of double strand breaks.

In conclusion, this study showed that the CRISPR/Cas9 method is a valuable tool to genetically modify mantle cell lymphoma cells. Potential disruptive factors of this method were identified and solutions were proposed. Moreover, it was validated that DLL4 acts as a potent stimulator for in vitro *NOTCH1* stimulation in mantle cell lymphoma.

Literature

1. Weisenburger DD, Kim H, Rappaport H. Mantle-zone lymphoma: a follicular variant of intermediate lymphocytic lymphoma. Cancer. 1982;49(7):1429-38.
2. Alaggio R, Amador C, Anagnostopoulos I, Attygalle AD, Araujo IBO, Berti E, et al. The 5th edition of the World Health Organization Classification of Haematolymphoid Tumours: Lymphoid Neoplasms. Leukemia. 2022;36(7):1720-48.
3. Dreyling M, editor. Seltene Lymphome. Epidemiologie - Diagnostik - Therapie: Georg Thieme Verlag; 2018.
4. Shankland KR, Armitage JO, Hancock BW. Non-Hodgkin lymphoma. Lancet. 2012;380(9844):848-57.
5. Klener P. Advances in Molecular Biology and Targeted Therapy of Mantle Cell Lymphoma. Int J Mol Sci. 2019;20(18).
6. Espinet B, Ferrer A, Bellosillo B, Nonell L, Salar A, Fernández-Rodríguez C, et al. Distinction between asymptomatic monoclonal B-cell lymphocytosis with cyclin D1 overexpression and mantle cell lymphoma: from molecular profiling to flow cytometry. Clin Cancer Res. 2014;20(4):1007-19.
7. Gao J, Peterson L, Nelson B, Goolsby C, Chen YH. Immunophenotypic variations in mantle cell lymphoma. Am J Clin Pathol. 2009;132(5):699-706.
8. Reddy P, Dabbas B, Gama M, Kocher T, Drum HL, Taylor J, et al. FMC-7 Expression Identifies Phenotypically Atypical Chronic Lymphocytic Leukemia with Distinct Clinical and Molecular Genetic Features. Blood. 2012;120(21):2478-.
9. Saksena A, Yin CC, Xu J, Li J, Zhou J, Wang SA, et al. CD23 expression in mantle cell lymphoma is associated with CD200 expression, leukemic non-nodal form, and a better prognosis. Hum Pathol. 2019;89:71-80.
10. Wang M, Sun L, Qian J, Han X, Zhang L, Lin P, et al. Cyclin D1 as a universally expressed mantle cell lymphoma-associated tumor antigen for immunotherapy. Leukemia. 2009;23(7):1320-8.
11. Li JY, Gaillard F, Moreau A, Harousseau JL, Laboisse C, Milpied N, et al. Detection of translocation t(11;14)(q13;q32) in mantle cell lymphoma by fluorescence in situ hybridization. Am J Pathol. 1999;154(5):1449-52.
12. Epperla N, Hamadani M, Fenske TS, Costa LJ. Incidence and survival trends in mantle cell lymphoma. Br J Haematol. 2018;181(5):703-6.
13. Sant M, Allemani C, Tereanu C, De Angelis R, Capocaccia R, Visser O, et al. Incidence of hematologic malignancies in Europe by morphologic subtype: results of the HAEMACARE project. Blood. 2010;116(19):3724-34.
14. Jares P, Colomer D, Campo E. Genetic and molecular pathogenesis of mantle cell lymphoma: perspectives for new targeted therapeutics. Nat Rev Cancer. 2007;7(10):750-62.
15. Jares P, Colomer D, Campo E. Molecular pathogenesis of mantle cell lymphoma. J Clin Invest. 2012;122(10):3416-23.
16. Banks PM, Chan J, Cleary ML, Delsol G, De Wolf-Peeters C, Gatter K, et al. Mantle cell lymphoma. A proposal for unification of morphologic, immunologic, and molecular data. Am J Surg Pathol. 1992;16(7):637-40.
17. Hunter T, Pines J. Cyclins and cancer. II: Cyclin D and CDK inhibitors come of age. Cell. 1994;79(4):573-82.
18. Malumbres M, Barbacid M. To cycle or not to cycle: a critical decision in cancer. Nat Rev Cancer. 2001;1(3):222-31.

19. Weinberg RA. The retinoblastoma protein and cell cycle control. Cell. 1995;81(3):323-30.
20. Bertoli C, Skotheim JM, de Bruin RA. Control of cell cycle transcription during G1 and S phases. Nat Rev Mol Cell Biol. 2013;14(8):518-28.
21. Kim JK, Diehl JA. Nuclear cyclin D1: an oncogenic driver in human cancer. J Cell Physiol. 2009;220(2):292-6.
22. Beà S, Valdés-Mas R, Navarro A, Salaverria I, Martín-Garcia D, Jares P, et al. Landscape of somatic mutations and clonal evolution in mantle cell lymphoma. Proc Natl Acad Sci U S A. 2013;110(45):18250-5.
23. Zhang J, Jima D, Moffitt AB, Liu Q, Czader M, Hsi ED, et al. The genomic landscape of mantle cell lymphoma is related to the epigenetically determined chromatin state of normal B cells. Blood. 2014;123(19):2988-96.
24. Pérez-Galán P, Dreyling M, Wiestner A. Mantle cell lymphoma: biology, pathogenesis, and the molecular basis of treatment in the genomic era. Blood. 2011;117(1):26-38.
25. Pararajalingam P, Coyle KM, Arthur SE, Thomas N, Alcaide M, Meissner B, et al. Coding and noncoding drivers of mantle cell lymphoma identified through exome and genome sequencing. Blood. 2020;136(5):572-84.
26. Fu K, Weisenburger DD, Greiner TC, Dave S, Wright G, Rosenwald A, et al. Cyclin D1-negative mantle cell lymphoma: a clinicopathologic study based on gene expression profiling. Blood. 2005;106(13):4315-21.
27. Mozos A, Royo C, Hartmann E, De Jong D, Baró C, Valera A, et al. SOX11 expression is highly specific for mantle cell lymphoma and identifies the cyclin D1-negative subtype. Haematologica. 2009;94(11):1555-62.
28. Narurkar R, Alkayem M, Liu D. SOX11 is a biomarker for cyclin D1-negative mantle cell lymphoma. Biomark Res. 2016;4:6.
29. Swerdlow SH, Campo E, Pileri SA, Harris NL, Stein H, Siebert R, et al. The 2016 revision of the World Health Organization classification of lymphoid neoplasms. Blood. 2016;127(20):2375-90.
30. Tiemann M, Schrader C, Klapper W, Dreyling MH, Campo E, Norton A, et al. Histopathology, cell proliferation indices and clinical outcome in 304 patients with mantle cell lymphoma (MCL): a clinicopathological study from the European MCL Network. Br J Haematol. 2005;131(1):29-38.
31. Welzel N, Le T, Marculescu R, Mitterbauer G, Chott A, Pott C, et al. Templated nucleotide addition and immunoglobulin JH-gene utilization in t(11;14) junctions: implications for the mechanism of translocation and the origin of mantle cell lymphoma. Cancer Res. 2001;61(4):1629-36.
32. Orchard J, Garand R, Davis Z, Babbage G, Sahota S, Matutes E, et al. A subset of t(11;14) lymphoma with mantle cell features displays mutated IgVH genes and includes patients with good prognosis, nonnodal disease. Blood. 2003;101(12):4975-81.
33. Samaha H, Dumontet C, Ketterer N, Moullet I, Thieblemont C, Bouafia F, et al. Mantle cell lymphoma: a retrospective study of 121 cases. Leukemia. 1998;12(8):1281-7.
34. Jain P, Wang M. Mantle cell lymphoma: 2019 update on the diagnosis, pathogenesis, prognostication, and management. Am J Hematol. 2019;94(6):710-25.
35. Dreyling M, Campo E, Hermine O, Jerkeman M, Le Gouill S, Rule S, et al. Newly diagnosed and relapsed mantle cell lymphoma: ESMO Clinical Practice Guidelines for diagnosis, treatment and follow-up. Ann Oncol. 2017;28(suppl_4):iv62-iv71.

36. Silkenstedt E, Hoster E, Bassermann F. Mantellzell-Lymphome. In: Dreyling M, editor. Manual Maligne Lymphome Empfehlungen zur Diagnostik, Therapie und Nachsorge. 11 ed. München: Zuckschwerdt Verlag; 2019.
37. Cheah CY, George A, Giné E, Chiappella A, Kluin-Nelemans HC, Jurczak W, et al. Central nervous system involvement in mantle cell lymphoma: clinical features, prognostic factors and outcomes from the European Mantle Cell Lymphoma Network. Ann Oncol. 2013;24(8):2119-23.
38. Carbone PP, Kaplan HS, Musshoff K, Smithers DW, Tubiana M. Report of the Committee on Hodgkin's Disease Staging Classification. Cancer Res. 1971;31(11):1860-1.
39. Herrmann A, Hoster E, Zwingers T, Brittinger G, Engelhard M, Meusers P, et al. Improvement of overall survival in advanced stage mantle cell lymphoma. J Clin Oncol. 2009;27(4):511-8.
40. Hoster E, Dreyling M, Klapper W, Gisselbrecht C, van Hoof A, Kluin-Nelemans HC, et al. A new prognostic index (MIPI) for patients with advanced-stage mantle cell lymphoma. Blood. 2008;111(2):558-65.
41. Hoster E, Klapper W, Hermine O, Kluin-Nelemans HC, Walewski J, van Hoof A, et al. Confirmation of the mantle-cell lymphoma International Prognostic Index in randomized trials of the European Mantle-Cell Lymphoma Network. J Clin Oncol. 2014;32(13):1338-46.
42. Yi S, Yan Y, Jin M, Bhattacharya S, Wang Y, Wu Y, et al. Genomic and transcriptomic profiling reveals distinct molecular subsets associated with outcomes in mantle cell lymphoma. J Clin Invest. 2022;132(3).
43. Aukema SM, Hoster E, Rosenwald A, Canoni D, Delfau-Larue MH, Rymkiewicz G, et al. Expression of TP53 is associated with the outcome of MCL independent of MIPI and Ki-67 in trials of the European MCL Network. Blood. 2018;131(4):417-20.
44. Wang ML, Jurczak W, Jerkeman M, Trotman J, Zinzani PL, Belada D, et al. Ibrutinib plus Bendamustine and Rituximab in Untreated Mantle-Cell Lymphoma. N Engl J Med. 2022;386(26):2482-94.
45. Abrisqueta P, Scott DW, Slack GW, Steidl C, Mottok A, Gascoyne RD, et al. Observation as the initial management strategy in patients with mantle cell lymphoma. Ann Oncol. 2017;28(10):2489-95.
46. Giné E, de la Cruz F, Jiménez Ubieto A, López Jimenez J, Martín García-Sancho A, Terol MJ, et al. Ibrutinib in Combination With Rituximab for Indolent Clinical Forms of Mantle Cell Lymphoma (IMCL-2015): A Multicenter, Open-Label, Single-Arm, Phase II Trial. J Clin Oncol. 2022;40(11):1196-205.
47. Hermine O, Jiang L, Walewski J, Bosly A, Thieblemont C, Szymczyk M, et al. High-Dose Cytarabine and Autologous Stem-Cell Transplantation in Mantle Cell Lymphoma: Long-Term Follow-Up of the Randomized Mantle Cell Lymphoma Younger Trial of the European Mantle Cell Lymphoma Network. J Clin Oncol. 2023;41(3):479-84.
48. Dreyling M, Lenz G, Hoster E, Van Hoof A, Gisselbrecht C, Schmits R, et al. Early consolidation by myeloablative radiochemotherapy followed by autologous stem cell transplantation in first remission significantly prolongs progression-free survival in mantle-cell lymphoma: results of a prospective randomized trial of the European MCL Network. Blood. 2005;105(7):2677-84.
49. Hoster E, Metzner B, Forstpointner R, Pfreundschuh M, Trümper L, Hallek M, et al. Autologous Stem Cell Transplantation and Addition of Rituximab Independently Prolong Response Duration in Advanced Stage Mantle Cell Lymphoma. Blood. 2009;114(22):880-.

50. Kumar A. What is the role of up-front autologous stem cell transplantation in mantle cell lymphoma? Hematology Am Soc Hematol Educ Program. 2022;2022(1):155-62.
51. Eskelund CW, Dahl C, Hansen JW, Westman M, Kolstad A, Pedersen LB, et al. TP53 mutations identify younger mantle cell lymphoma patients who do not benefit from intensive chemoimmunotherapy. Blood. 2017;130(17):1903-10.
52. Le Gouill S, Thieblemont C, Oberic L, Moreau A, Bouabdallah K, Dartigeas C, et al. Rituximab after Autologous Stem-Cell Transplantation in Mantle-Cell Lymphoma. N Engl J Med. 2017;377(13):1250-60.
53. Rozental A, Jim HSL, Extermann M. Treatment of older patients with mantle cell lymphoma in the era of novel agents. Leuk Lymphoma. 2023;64(9):1514-26.
54. Robak T, Jin J, Pylypenko H, Verhoef G, Siritanaratkul N, Drach J, et al. Frontline bortezomib, rituximab, cyclophosphamide, doxorubicin, and prednisone (VR-CAP) versus rituximab, cyclophosphamide, doxorubicin, vincristine, and prednisone (R-CHOP) in transplantation-ineligible patients with newly diagnosed mantle cell lymphoma: final overall survival results of a randomised, open-label, phase 3 study. Lancet Oncol. 2018;19(11):1449-58.
55. Visco C, Chiappella A, Nassi L, Patti C, Ferrero S, Barbero D, et al. Rituximab, bendamustine, and low-dose cytarabine as induction therapy in elderly patients with mantle cell lymphoma: a multicentre, phase 2 trial from Fondazione Italiana Linfomi. Lancet Haematol. 2017;4(1):e15-e23.
56. Rummel MJ, Niederle N, Maschmeyer G, Banat GA, von Grünhagen U, Losem C, et al. Bendamustine plus rituximab versus CHOP plus rituximab as first-line treatment for patients with indolent and mantle-cell lymphomas: an open-label, multicentre, randomised, phase 3 non-inferiority trial. Lancet. 2013;381(9873):1203-10.
57. Kluin-Nelemans HC, Hoster E, Hermine O, Walewski J, Trneny M, Geisler CH, et al. Treatment of older patients with mantle-cell lymphoma. N Engl J Med. 2012;367(6):520-31.
58. Wang ML, Rule S, Martin P, Goy A, Auer R, Kahl BS, et al. Targeting BTK with ibrutinib in relapsed or refractory mantle-cell lymphoma. N Engl J Med. 2013;369(6):507-16.
59. Martin P, Maddocks K, Leonard JP, Ruan J, Goy A, Wagner-Johnston N, et al. Postibrutinib outcomes in patients with mantle cell lymphoma. Blood. 2016;127(12):1559-63.
60. Jiang H, Lwin T, Zhao X, Ren Y, Li G, Moscinski L, et al. Venetoclax as a single agent and in combination with PI3K-MTOR1/2 kinase inhibitors against ibrutinib sensitive and resistant mantle cell lymphoma. Br J Haematol. 2019;184(2):298-302.
61. Trněný M, Lamy T, Walewski J, Belada D, Mayer J, Radford J, et al. Lenalidomide versus investigator's choice in relapsed or refractory mantle cell lymphoma (MCL-002; SPRINT): a phase 2, randomised, multicentre trial. Lancet Oncol. 2016;17(3):319-31.
62. Robinson S, Dreger P, Caballero D, Corradini P, Geisler C, Ghielmini M, et al. The EBMT/EMCL consensus project on the role of autologous and allogeneic stem cell transplantation in mantle cell lymphoma. Leukemia. 2015;29(2):464-73.
63. Wang M, Munoz J, Goy A, Locke FL, Jacobson CA, Hill BT, et al. KTE-X19 CAR T-Cell Therapy in Relapsed or Refractory Mantle-Cell Lymphoma. New England Journal of Medicine. 2020;382(14):1331-42.
64. Munshi PN, Hamadani M, Kumar A, Dreger P, Friedberg JW, Dreyling M, et al. American Society of Transplantation and Cellular Therapy, Center of International Blood and Marrow Transplant Research, and European Society for Blood and Marrow

Transplantation Clinical Practice Recommendations for Transplantation and Cellular Therapies in Mantle Cell Lymphoma. Transplant Cell Ther. 2021;27(9):720-8.
65. Bray SJ. Notch signalling: a simple pathway becomes complex. Nat Rev Mol Cell Biol. 2006;7(9):678-89.
66. Mumm JS, Schroeter EH, Saxena MT, Griesemer A, Tian X, Pan DJ, et al. A ligand-induced extracellular cleavage regulates gamma-secretase-like proteolytic activation of Notch1. Mol Cell. 2000;5(2):197-206.
67. Brou C, Logeat F, Gupta N, Bessia C, LeBail O, Doedens JR, et al. A novel proteolytic cleavage involved in Notch signaling: the role of the disintegrin-metalloprotease TACE. Mol Cell. 2000;5(2):207-16.
68. Fortini ME. Gamma-secretase-mediated proteolysis in cell-surface-receptor signalling. Nat Rev Mol Cell Biol. 2002;3(9):673-84.
69. Maillard I, Fang T, Pear WS. Regulation of lymphoid development, differentiation, and function by the Notch pathway. Annu Rev Immunol. 2005;23:945-74.
70. Arruga F, Vaisitti T, Deaglio S. The NOTCH Pathway and Its Mutations in Mature B Cell Malignancies. Front Oncol. 2018;8:550.
71. Hadland BK, Huppert SS, Kanungo J, Xue Y, Jiang R, Gridley T, et al. A requirement for Notch1 distinguishes 2 phases of definitive hematopoiesis during development. Blood. 2004;104(10):3097-105.
72. Thompson BJ, Buonamici S, Sulis ML, Palomero T, Vilimas T, Basso G, et al. The SCFFBW7 ubiquitin ligase complex as a tumor suppressor in T cell leukemia. J Exp Med. 2007;204(8):1825-35.
73. Lubman OY, Korolev SV, Kopan R. Anchoring notch genetics and biochemistry; structural analysis of the ankyrin domain sheds light on existing data. Mol Cell. 2004;13(5):619-26.
74. Fryer CJ, White JB, Jones KA. Mastermind recruits CycC:CDK8 to phosphorylate the Notch ICD and coordinate activation with turnover. Mol Cell. 2004;16(4):509-20.
75. Kridel R, Meissner B, Rogic S, Boyle M, Telenius A, Woolcock B, et al. Whole transcriptome sequencing reveals recurrent NOTCH1 mutations in mantle cell lymphoma. Blood. 2012;119(9):1963-71.
76. Malecki MJ, Sanchez-Irizarry C, Mitchell JL, Histen G, Xu ML, Aster JC, et al. Leukemia-associated mutations within the NOTCH1 heterodimerization domain fall into at least two distinct mechanistic classes. Mol Cell Biol. 2006;26(12):4642-51.
77. Yang P, Liu SZ, Li CY, Zhang WL, Wang J, Chen YT, et al. Genetic and prognostic analysis of blastoid and pleomorphic mantle cell lymphoma: a multicenter analysis in China. Ann Hematol. 2024.
78. Arruga F, Bracciamà V, Vitale N, Vaisitti T, Gizzi K, Yeomans A, et al. Bidirectional linkage between the B-cell receptor and NOTCH1 in chronic lymphocytic leukemia and in Richter's syndrome: therapeutic implications. Leukemia. 2020;34(2):462-77.
79. Puente XS, Pinyol M, Quesada V, Conde L, Ordóñez GR, Villamor N, et al. Whole-genome sequencing identifies recurrent mutations in chronic lymphocytic leukaemia. Nature. 2011;475(7354):101-5.
80. Rossi D, Rasi S, Fabbri G, Spina V, Fangazio M, Forconi F, et al. Mutations of NOTCH1 are an independent predictor of survival in chronic lymphocytic leukemia. Blood. 2012;119(2):521-9.
81. Weng AP, Ferrando AA, Lee W, Morris JPt, Silverman LB, Sanchez-Irizarry C, et al. Activating mutations of NOTCH1 in human T cell acute lymphoblastic leukemia. Science. 2004;306(5694):269-71.

82. Tyagi A, Sharma AK, Damodaran C. A Review on Notch Signaling and Colorectal Cancer. Cells. 2020;9(6).
83. Leong KG, Gao WQ. The Notch pathway in prostate development and cancer. Differentiation. 2008;76(6):699-716.
84. Yuan X, Zhang M, Wu H, Xu H, Han N, Chu Q, et al. Expression of Notch1 Correlates with Breast Cancer Progression and Prognosis. PLoS One. 2015;10(6):e0131689.
85. Balint K, Xiao M, Pinnix CC, Soma A, Veres I, Juhasz I, et al. Activation of Notch1 signaling is required for beta-catenin-mediated human primary melanoma progression. J Clin Invest. 2005;115(11):3166-76.
86. Zheng R, Li M, Wang S, Liu Y. Advances of target therapy on NOTCH1 signaling pathway in T-cell acute lymphoblastic leukemia. Experimental Hematology & Oncology. 2020;9(1):31.
87. Cullion K, Draheim KM, Hermance N, Tammam J, Sharma VM, Ware C, et al. Targeting the Notch1 and mTOR pathways in a mouse T-ALL model. Blood. 2009;113(24):6172-81.
88. López-Guerra M, Xargay-Torrent S, Rosich L, Montraveta A, Roldán J, Matas-Céspedes A, et al. The γ-secretase inhibitor PF-03084014 combined with fludarabine antagonizes migration, invasion and angiogenesis in NOTCH1-mutated CLL cells. Leukemia. 2015;29(1):96-106.
89. Ma S, Xu J, Wang X, Wu QY, Cao J, Li ZY, et al. [Effect of ADAM10 Inhibitor GI254023X on Proliferation and Apoptosis of Acute T-Lymphoblastic Leukemia Jurkat Cells In Vitro and Its Possible Mechanisms]. Zhongguo Shi Yan Xue Ye Xue Za Zhi. 2015;23(4):950-5.
90. Valentina A, Sonia M, Marica P, Alessandra G, Laura P, Adriana Agnese A, et al. Dissecting molecular mechanisms of resistance to NOTCH1-targeted therapy in T-cell acute lymphoblastic leukemia xenografts. Haematologica. 2020;105(5):1317-28.
91. Sharma A, Gadkari RA, Ramakanth SV, Padmanabhan K, Madhumathi DS, Devi L, et al. A novel Monoclonal Antibody against Notch1 Targets Leukemia-associated Mutant Notch1 and Depletes Therapy Resistant Cancer Stem Cells in Solid Tumors. Sci Rep. 2015;5:11012.
92. Silkenstedt E, Arenas F, Colom-Sanmarti B, Xargay-Torrent S, Higashi M, Giro A, et al. Notch1 signaling in NOTCH1-mutated mantle cell lymphoma depends on Delta-Like ligand 4 and is a potential target for specific antibody therapy. J Exp Clin Cancer Res. 2019;38(1):446.
93. Barrangou R, Fremaux C, Deveau H, Richards M, Boyaval P, Moineau S, et al. CRISPR provides acquired resistance against viruses in prokaryotes. Science. 2007;315(5819):1709-12.
94. Makarova KS, Haft DH, Barrangou R, Brouns SJ, Charpentier E, Horvath P, et al. Evolution and classification of the CRISPR-Cas systems. Nat Rev Microbiol. 2011;9(6):467-77.
95. Cong L, Ran FA, Cox D, Lin S, Barretto R, Habib N, et al. Multiplex genome engineering using CRISPR/Cas systems. Science. 2013;339(6121):819-23.
96. Cox DB, Platt RJ, Zhang F. Therapeutic genome editing: prospects and challenges. Nat Med. 2015;21(2):121-31.
97. Jinek M, Chylinski K, Fonfara I, Hauer M, Doudna JA, Charpentier E. A programmable dual-RNA-guided DNA endonuclease in adaptive bacterial immunity. Science. 2012;337(6096):816-21.

98. Urnov FD, Rebar EJ, Holmes MC, Zhang HS, Gregory PD. Genome editing with engineered zinc finger nucleases. Nat Rev Genet. 2010;11(9):636-46.
99. Bogdanove AJ, Voytas DF. TAL effectors: customizable proteins for DNA targeting. Science. 2011;333(6051):1843-6.
100. Whitworth KM, Rowland RR, Ewen CL, Trible BR, Kerrigan MA, Cino-Ozuna AG, et al. Gene-edited pigs are protected from porcine reproductive and respiratory syndrome virus. Nat Biotechnol. 2016;34(1):20-2.
101. Zhu H, Li C, Gao C. Applications of CRISPR-Cas in agriculture and plant biotechnology. Nat Rev Mol Cell Biol. 2020;21(11):661-77.
102. Zeng Y, Wen J, Zhao W, Wang Q, Huang W. Rational Improvement of Rice Yield and Cold Tolerance by Editing the Three Genes OsPIN5b, GS3, and OsMYB30 With the CRISPR-Cas9 System. Front Plant Sci. 2019;10:1663.
103. Sánchez-León S, Gil-Humanes J, Ozuna CV, Giménez MJ, Sousa C, Voytas DF, et al. Low-gluten, nontransgenic wheat engineered with CRISPR/Cas9. Plant Biotechnol J. 2018;16(4):902-10.
104. Li JR, Walker S, Nie JB, Zhang XQ. Experiments that led to the first gene-edited babies: the ethical failings and the urgent need for better governance. J Zhejiang Univ Sci B. 2019;20(1):32-8.
105. Ledford H. CRISPR babies: when will the world be ready? Nature. 2019;570(7761):293-6.
106. Cyranoski D. The CRISPR-baby scandal: what's next for human gene-editing. Nature. 2019;566(7745):440-2.
107. De Miguel Beriain I. Is the 'serious' factor in germline modification really relevant? A response to Kleiderman, Ravitsky and Knoppers. J Med Ethics. 2020;46(2):151-2.
108. Pardo B, Gómez-González B, Aguilera A. DNA repair in mammalian cells: DNA double-strand break repair: how to fix a broken relationship. Cell Mol Life Sci. 2009;66(6):1039-56.
109. Rothkamm K, Krüger I, Thompson LH, Löbrich M. Pathways of DNA double-strand break repair during the mammalian cell cycle. Mol Cell Biol. 2003;23(16):5706-15.
110. Moore JK, Haber JE. Cell cycle and genetic requirements of two pathways of nonhomologous end-joining repair of double-strand breaks in Saccharomyces cerevisiae. Mol Cell Biol. 1996;16(5):2164-73.
111. Zhao X, Wei C, Li J, Xing P, Li J, Zheng S, et al. Cell cycle-dependent control of homologous recombination. Acta Biochim Biophys Sin (Shanghai). 2017;49(8):655-68.
112. Porteus MH. Towards a new era in medicine: therapeutic genome editing. Genome Biol. 2015;16:286.
113. Koo T, Lee J, Kim JS. Measuring and Reducing Off-Target Activities of Programmable Nucleases Including CRISPR-Cas9. Mol Cells. 2015;38(6):475-81.
114. Kim D, Bae S, Park J, Kim E, Kim S, Yu HR, et al. Digenome-seq: genome-wide profiling of CRISPR-Cas9 off-target effects in human cells. Nat Methods. 2015;12(3):237-43, 1 p following 43.
115. Xie F, Ye L, Chang JC, Beyer AI, Wang J, Muench MO, et al. Seamless gene correction of β-thalassemia mutations in patient-specific iPSCs using CRISPR/Cas9 and piggyBac. Genome Res. 2014;24(9):1526-33.
116. Demirci S, Leonard A, Haro-Mora JJ, Uchida N, Tisdale JF. CRISPR/Cas9 for Sickle Cell Disease: Applications, Future Possibilities, and Challenges. Adv Exp Med Biol. 2019;1144:37-52.

117. Morishige S, Mizuno S, Ozawa H, Nakamura T, Mazahery A, Nomura K, et al. CRISPR/Cas9-mediated gene correction in hemophilia B patient-derived iPSCs. Int J Hematol. 2020;111(2):225-33.
118. Tian X, Gu T, Patel S, Bode AM, Lee MH, Dong Z. CRISPR/Cas9 - An evolving biological tool kit for cancer biology and oncology. NPJ Precis Oncol. 2019;3:8.
119. Lu Y, Xue J, Deng T, Zhou X, Yu K, Deng L, et al. Safety and feasibility of CRISPR-edited T cells in patients with refractory non-small-cell lung cancer. Nat Med. 2020;26(5):732-40.
120. Stadtmauer EA, Fraietta JA, Davis MM, Cohen AD, Weber KL, Lancaster E, et al. CRISPR-engineered T cells in patients with refractory cancer. Science. 2020;367(6481).
121. Beyar-Katz O, Gill S. Advances in chimeric antigen receptor T cells. Curr Opin Hematol. 2020;27(6):368-77.
122. Liu Y, Chen X, Han W, Zhang Y. Tisagenlecleucel, an approved anti-CD19 chimeric antigen receptor T-cell therapy for the treatment of leukemia. Drugs Today (Barc). 2017;53(11):597-608.
123. Abramson JS. Anti-CD19 CAR T-Cell Therapy for B-Cell Non-Hodgkin Lymphoma. Transfus Med Rev. 2020;34(1):29-33.
124. Neelapu SS, Tummala S, Kebriaei P, Wierda W, Gutierrez C, Locke FL, et al. Chimeric antigen receptor T-cell therapy - assessment and management of toxicities. Nat Rev Clin Oncol. 2018;15(1):47-62.
125. Nie EH, Su YJ, Baird JH, Agarwal N, Bharadwaj S, Weng WK, et al. Clinical Features of Neurotoxicity Following CD19 CAR T-cell Therapy in Mantle Cell Lymphoma. Blood Adv. 2024.
126. Xu L, Wang J, Liu Y, Xie L, Su B, Mou D, et al. CRISPR-Edited Stem Cells in a Patient with HIV and Acute Lymphocytic Leukemia. N Engl J Med. 2019;381(13):1240-7.
127. Ebina H, Misawa N, Kanemura Y, Koyanagi Y. Harnessing the CRISPR/Cas9 system to disrupt latent HIV-1 provirus. Sci Rep. 2013;3:2510.
128. Min YL, Bassel-Duby R, Olson EN. CRISPR Correction of Duchenne Muscular Dystrophy. Annu Rev Med. 2019;70:239-55.
129. Li HL, Fujimoto N, Sasakawa N, Shirai S, Ohkame T, Sakuma T, et al. Precise correction of the dystrophin gene in duchenne muscular dystrophy patient induced pluripotent stem cells by TALEN and CRISPR-Cas9. Stem Cell Reports. 2015;4(1):143-54.
130. Nelson CE, Hakim CH, Ousterout DG, Thakore PI, Moreb EA, Castellanos Rivera RM, et al. In vivo genome editing improves muscle function in a mouse model of Duchenne muscular dystrophy. Science. 2016;351(6271):403-7.
131. Aoki Y, Yokota T, Nagata T, Nakamura A, Tanihata J, Saito T, et al. Bodywide skipping of exons 45-55 in dystrophic mdx52 mice by systemic antisense delivery. Proc Natl Acad Sci U S A. 2012;109(34):13763-8.
132. Lai R, McDonnell TJ, O'Connor SL, Medeiros LJ, Oudat R, Keating M, et al. Establishment and characterization of a new mantle cell lymphoma cell line, Mino. Leuk Res. 2002;26(9):849-55.
133. Jeon HJ, Kim CW, Yoshino T, Akagi T. Establishment and characterization of a mantle cell lymphoma cell line. Br J Haematol. 1998;102(5):1323-6.
134. Amin HM, McDonnell TJ, Medeiros LJ, Rassidakis GZ, Leventaki V, O'Connor SL, et al. Characterization of 4 mantle cell lymphoma cell lines. Arch Pathol Lab Med. 2003;127(4):424-31.
135. Doench JG, Fusi N, Sullender M, Hegde M, Vaimberg EW, Donovan KF, et al. Optimized sgRNA design to maximize activity and minimize off-target effects of CRISPR-Cas9. Nat Biotechnol. 2016;34(2):184-91.

136. BIOIMAGING BDLDBIHB. Protocol for Rapid and Versatile Genome Engineering Using The MIN (Multifunctional Integrase) Strategy https://human.bio.lmu.de/_webtools/MINtool/MINTagging_Protocol.pdf [
137. Brinkman EK, Chen T, Amendola M, van Steensel B. Easy quantitative assessment of genome editing by sequence trace decomposition. Nucleic Acids Res. 2014;42(22):e168.
138. McCaw TR, Inga E, Chen H, Jaskula-Sztul R, Dudeja V, Bibb JA, et al. Gamma Secretase Inhibitors in Cancer: A Current Perspective on Clinical Performance. Oncologist. 2021;26(4):e608-e21.
139. Xie M, Wei S, Wu X, Li X, You Y, He C. Alterations of Notch pathway in patients with adenoid cystic carcinoma of the trachea and its impact on survival. Lung Cancer. 2018;121:41-7.
140. Agnusdei V, Minuzzo S, Frasson C, Grassi A, Axelrod F, Satyal S, et al. Therapeutic antibody targeting of Notch1 in T-acute lymphoblastic leukemia xenografts. Leukemia. 2014;28(2):278-88.
141. Jacquemin V, Antoine M, Dom G, Detours V, Maenhaut C, Dumont JE. Dynamic Cancer Cell Heterogeneity: Diagnostic and Therapeutic Implications. Cancers (Basel). 2022;14(2).
142. Che Y, Liu Y, Yao Y, Hill HA, Li Y, Cai Q, et al. Exploiting PRMT5 as a target for combination therapy in mantle cell lymphoma characterized by frequent ATM and TP53 mutations. Blood Cancer J. 2023;13(1):27.
143. Haeussler M, Schönig K, Eckert H, Eschstruth A, Mianné J, Renaud J-B, et al. Evaluation of off-target and on-target scoring algorithms and integration into the guide RNA selection tool CRISPOR. Genome Biology. 2016;17(1):148.
144. Zhang XH, Tee LY, Wang XG, Huang QS, Yang SH. Off-target Effects in CRISPR/Cas9-mediated Genome Engineering. Mol Ther Nucleic Acids. 2015;4(11):e264.
145. Fu Y, Foden JA, Khayter C, Maeder ML, Reyon D, Joung JK, et al. High-frequency off-target mutagenesis induced by CRISPR-Cas nucleases in human cells. Nat Biotechnol. 2013;31(9):822-6.
146. Russell DW, Hirata RK. Human gene targeting by viral vectors. Nat Genet. 1998;18(4):325-30.
147. Gaj T, Epstein BE, Schaffer DV. Genome Engineering Using Adeno-associated Virus: Basic and Clinical Research Applications. Mol Ther. 2016;24(3):458-64.
148. Lee K, Mackley VA, Rao A, Chong AT, Dewitt MA, Corn JE, et al. Synthetically modified guide RNA and donor DNA are a versatile platform for CRISPR-Cas9 engineering. eLife. 2017;6:e25312.
149. Robert F, Barbeau M, Éthier S, Dostie J, Pelletier J. Pharmacological inhibition of DNA-PK stimulates Cas9-mediated genome editing. Genome Med. 2015;7(1):93.
150. Weterings E, Gallegos AC, Dominick LN, Cooke LS, Bartels TN, Vagner J, et al. A novel small molecule inhibitor of the DNA repair protein Ku70/80. DNA Repair (Amst). 2016;43:98-106.
151. Yu C, Liu Y, Ma T, Liu K, Xu S, Zhang Y, et al. Small molecules enhance CRISPR genome editing in pluripotent stem cells. Cell Stem Cell. 2015;16(2):142-7.
152. Nambiar TS, Billon P, Diedenhofen G, Hayward SB, Taglialatela A, Cai K, et al. Stimulation of CRISPR-mediated homology-directed repair by an engineered RAD18 variant. Nature Communications. 2019;10(1):3395.
153. Fus-Kujawa A, Prus P, Bajdak-Rusinek K, Teper P, Gawron K, Kowalczuk A, et al. An Overview of Methods and Tools for Transfection of Eukaryotic Cells in vitro. Front Bioeng Biotechnol. 2021;9:701031.

154. Piñero J, López-Baena M, Ortiz T, Cortés F. Apoptotic and necrotic cell death are both induced by electroporation in HL60 human promyeloid leukaemia cells. Apoptosis. 1997;2(3):330-6.
155. Jordan ET, Collins M, Terefe J, Ugozzoli L, Rubio T. Optimizing electroporation conditions in primary and other difficult-to-transfect cells. J Biomol Tech. 2008;19(5):328-34.
156. Box A, DeLay M, Tighe S, Chittur SV, Bergeron A, Cochran M, et al. Evaluating the Effects of Cell Sorting on Gene Expression. J Biomol Tech. 2020;31(3):100-11.
157. Llufrio EM, Wang L, Naser FJ, Patti GJ. Sorting cells alters their redox state and cellular metabolome. Redox Biol. 2018;16:381-7.
158. Box A, Holmes L, DeLay M, Adams D, Bergeron A, Clise-Dwyer K, et al. Cell Sorter Cleaning Practices and Their Impact on Instrument Sterility. J Biomol Tech. 2022;33(1).
159. Munoz A, Morachis JM. High efficiency sorting and outgrowth for single-cell cloning of mammalian cell lines. Biotechnol Lett. 2022;44(11):1337-46.
160. Heeneman S, Deutz NE, Buurman WA. The concentrations of glutamine and ammonia in commercially available cell culture media. J Immunol Methods. 1993;166(1):85-91.
161. Kawamoto-Miyamoto N, Hosoda H, Miyoshi K, Nomoto K. Glutamate in the medium of Lactiplantibacillus plantarum FL-664 affects the production of IL-12(p40) on murine spleen cells. Biosci Biotechnol Biochem. 2022;86(4):535-42.
162. Haas HS, Pfragner R, Siegl V, Ingolic E, Heintz E, Schauenstein K. Glutamate receptor-mediated effects on growth and morphology of human histiocytic lymphoma cells. Int J Oncol. 2005;27(3):867-74.
163. Good NE, Izawa S. Hydrogen ion buffers. Methods Enzymol. 1972;24:53-68.
164. Williamson JD, Cox P. Use of a new buffer in the culture of animal cells. J Gen Virol. 1968;2(2):309-12.
165. Porter AM, Macaulay RJ. STUDIES ON FLOCCULATION: I. A RELATIONSHIP BETWEEN THE pH AND CALCIUM CONTENT OF THE GROWTH MEDIUM. Journal of the Institute of Brewing. 1965;71(2):175-9.
166. Belhaj K, Chaparro-Garcia A, Kamoun S, Patron NJ, Nekrasov V. Editing plant genomes with CRISPR/Cas9. Curr Opin Biotechnol. 2015;32:76-84.
167. Manghwar H, Li B, Ding X, Hussain A, Lindsey K, Zhang X, et al. CRISPR/Cas Systems in Genome Editing: Methodologies and Tools for sgRNA Design, Off-Target Evaluation, and Strategies to Mitigate Off-Target Effects. Adv Sci (Weinh). 2020;7(6):1902312.
168. Uniyal AP, Mansotra K, Yadav SK, Kumar V. An overview of designing and selection of sgRNAs for precise genome editing by the CRISPR-Cas9 system in plants. 3 Biotech. 2019;9(6):223.
169. Komor AC, Badran AH, Liu DR. Editing the Genome Without Double-Stranded DNA Breaks. ACS Chem Biol. 2018;13(2):383-8.
170. Slesarenko YS, Lavrov AV, Smirnikhina SA. Off-target effects of base editors: what we know and how we can reduce it. Curr Genet. 2022;68(1):39-48.
171. Slaymaker IM, Gao L, Zetsche B, Scott DA, Yan WX, Zhang F. Rationally engineered Cas9 nucleases with improved specificity. Science. 2016;351(6268):84-8.
172. Kleinstiver BP, Pattanayak V, Prew MS, Tsai SQ, Nguyen NT, Zheng Z, et al. High-fidelity CRISPR-Cas9 nucleases with no detectable genome-wide off-target effects. Nature. 2016;529(7587):490-5.
173. Sade H, Krishna S, Sarin A. The anti-apoptotic effect of Notch-1 requires p56lck-dependent, Akt/PKB-mediated signaling in T cells. J Biol Chem. 2004;279(4):2937-44.

174. Benedetti D, Tissino E, Pozzo F, Bittolo T, Caldana C, Perini C, et al. NOTCH1 mutations are associated with high CD49d expression in chronic lymphocytic leukemia: link between the NOTCH1 and the NF-κB pathways. Leukemia. 2018;32(3):654-62.
175. Jang MS, Miao H, Carlesso N, Shelly L, Zlobin A, Darack N, et al. Notch-1 regulates cell death independently of differentiation in murine erythroleukemia cells through multiple apoptosis and cell cycle pathways. J Cell Physiol. 2004;199(3):418-33.
176. Wienert B, Shin J, Zelin E, Pestal K, Corn JE. In vitro-transcribed guide RNAs trigger an innate immune response via the RIG-I pathway. PLoS Biol. 2018;16(7):e2005840.
177. Álvarez MM, Biayna J, Supek F. TP53-dependent toxicity of CRISPR/Cas9 cuts is differential across genomic loci and can confound genetic screening. Nature Communications. 2022;13(1):4520.
178. Haapaniemi E, Botla S, Persson J, Schmierer B, Taipale J. CRISPR–Cas9 genome editing induces a p53-mediated DNA damage response. Nature Medicine. 2018;24(7):927-30.
179. Bowden AR, Morales-Juarez DA, Sczaniecka-Clift M, Agudo MM, Lukashchuk N, Thomas JC, et al. Parallel CRISPR-Cas9 screens clarify impacts of p53 on screen performance. Elife. 2020;9.
180. Xia C, Sadeghi L, Strååt K, Merrien M, Wright AP, Sander B, et al. Intrinsic 5-lipoxygenase activity regulates migration and adherence of mantle cell lymphoma cells. Prostaglandins Other Lipid Mediat. 2021;156:106575.
181. Song B, Yang S, Hwang GH, Yu J, Bae S. Analysis of NHEJ-Based DNA Repair after CRISPR-Mediated DNA Cleavage. Int J Mol Sci. 2021;22(12).
182. Schneider Y, Turan S, Koller A, Krumbiegel M, Farrell M, Plötz S, et al. Generation of a homozygous and a heterozygous SNCA gene knockout human-induced pluripotent stem cell line by CRISPR/Cas9 mediated allele-specific tuning of SNCA expression. Stem Cell Res. 2022;65:102952.
183. Evans K, Albanetti T, Venkat R, Schoner R, Savery J, Miro-Quesada G, et al. Assurance of monoclonality in one round of cloning through cell sorting for single cell deposition coupled with high resolution cell imaging. Biotechnol Prog. 2015;31(5):1172-8.
184. López-Guerra M, Xargay-Torrent S, Fuentes P, Roldán J, González-Farré B, Rosich L, et al. Specific NOTCH1 antibody targets DLL4-induced proliferation, migration, and angiogenesis in NOTCH1-mutated CLL cells. Oncogene. 2020;39(6):1185-97.

Acknowledgments

I would like to thank Prof. Dr. med. Martin Dreyling for granting me the opportunity of this thesis, as well as for his guidance and support throughout this project. It was a privilege to be a part of AG Dreyling and the ELLF (experimentelle Leukämie- und Lymphomforschung) laboratory.

I would also like to thank Dr. med. Elisabeth Silkenstedt for her mentorship during this project, William D. Keay for assisting me with new methods and Yvonne Zimmermann for her invaluable instructions, preparations and assistance she provided for my experiments. I am also grateful to all those who have contributed in any way to the completion of this thesis; your support has been truly appreciated.

Finally, I express a major appreciation to my family, from which I never got anything less than their full support throughout this journey.

Eidesstattliche Versicherung

Eidesstattliche Versicherung

DONVEN, Martine

Name, Vorname

Ich erkläre hiermit an Eides statt, dass ich die vorliegende Dissertation mit dem Titel:

CRISPR/Cas9-mediated gene editing to analyze the impact of *NOTCH1* mutations and their potential as a therapeutic target in mantle cell lymphoma

selbständig verfasst, mich außer der angegebenen keiner weiteren Hilfsmittel bedient und alle Erkenntnisse, die aus dem Schrifttum ganz oder annähernd übernommen sind, als solche kenntlich gemacht und nach ihrer Herkunft unter Bezeichnung der Fundstelle einzeln nachgewiesen habe.

Ich erkläre des Weiteren, dass die hier vorgelegte Dissertation nicht in gleicher oder in ähnlicher Form bei einer anderen Stelle zur Erlangung eines akademischen Grades eingereicht wurde.

München, den 25.07.2025 — DONVEN Martine

Ort, Datum — Unterschrift Doktorandin bzw. Doktorand

Erklärung zur Übereinstimmung der gebundenen Ausgabe der Dissertation mit der elektronischen Fassung

Erklärung zur Übereinstimmung der gebundenen Ausgabe der Dissertation mit der elektronischen Fassung

DONVEN, Martine

Name, Vorname

Hiermit erkläre ich, dass die elektronische Version der eingereichten Dissertation mit dem Titel:

CRISPR/Cas9-mediated gene editing to analyze the impact of *NOTCH1* mutations and their potential as a therapeutic target in mantle cell lymphoma

in Inhalt und Formatierung mit den gedruckten und gebundenen Exemplaren übereinstimmt.

Ich erkläre des Weiteren, dass die hier vorgelegte Dissertation nicht in gleicher oder in ähnlicher Form bei einer anderen Stelle zur Erlangung eines akademischen Grades eingereicht wurde.

München, den 25.07.2025 — DONVEN Martine

Ort, Datum — Unterschrift Doktorandin bzw. Doktorand